

Jet flipping and scouring characteristics by 2-D wall jets

Er, Jenn Wei.

2012

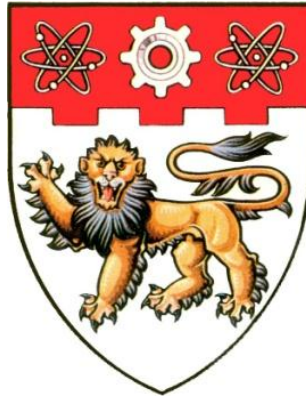
Er, J. W. (2012). Jet flipping and scouring characteristics by 2-D wall jets. Final year project report, Nanyang Technological University.

<https://hdl.handle.net/10356/95509>

Nanyang Technological University

Downloaded on 13 Mar 2024 18:31:59 SGT

JET FLIPPING AND SCOURING CHARACTERISTICS BY 2-D WALL JETS



ER JENN WEI

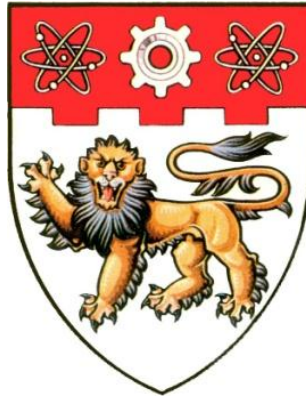
SCHOOL OF CIVIL AND ENVIRONMENTAL ENGINEERING

COLLEGE OF ENGINEERING

NANYANG TECHNOLOGICAL UNIVERSITY

2011/2012

JET FLIPPING AND SCOURING CHARACTERISTICS BY 2-D WALL JETS



ER JENN WEI

SCHOOL OF CIVIL AND ENVIRONMENTAL ENGINEERING

COLLEGE OF ENGINEERING

NANYANG TECHNOLOGICAL UNIVERSITY

2011/2012

**A Final Year Project presented to the Nanyang Technological University
in partial fulfillment of the requirements for the
Degree of Bachelor of Engineering**

2011/2012

ABSTRACT

In this project, the result of an experimental investigation on scour of non-cohesive and uniform sediment beds downstream of a sluice gate, due to a submerged two-dimensional wall jets issuing from a sluice opening were presented. All the experiments were conducted under high flow submergence with or without an apron. The jet issued from the sluice gate and impinging on an erodible bed can produce two very different flow patterns, depending on the experimental conditions. The observations and characteristics of the sediment bed downstream of the sluice gate during the scouring process was being described and explained in this report.

The first is a bed jet where the jet always impinges towards the sediment bed with digging action occurring at the sediment bed. The second is a surface jet where the jet axis points towards the water surface after issuing from the sluice gate. The second flow pattern may drag the sediments in the downstream side of the scoured zone back to the upstream filling up the scour hole in the process. However, it also caused the maximum scour depth to be located closer to the sluice structure which may impose greater threat than the bed jet. These two flow patterns, i.e., digging with bed jet and filing with surface jet, occur alternatively and over many dig-fill cycles throughout the duration of the scouring process.

The results on the effect of the apron length on the jet flipping phenomenon showed that the duration of the filling phase is generally longer than the digging phase with longer apron length. The duration to complete one dig-fill cycle also decreases with increases in apron length. For apron length as a ratio of the jet opening, L/d_o greater than 35, there is no jet flipping and only bed jet was observed. Similarly, when there is no apron, i.e., L/d_o is equal to zero, there is no jet flipping in the scour hole.

Based on the results, it was found that generally the maximum scour depth, d_{se-dig} during the digging phase and minimum scour depth, $d_{se-fill}$ during the filling phase increase as the apron length decreases. The difference between the d_{se-dig} and $d_{se-fill}$ is larger with increases in jet discharge. At the downstream of the scour hole, the sand ridge formed is affected by the cyclical digging and filling action. There are two sand ridges formed with different heights during the dig-fill cycles. For apron length ratio, L/d_o lower than 2, the height of sand ridge during the filling phase is higher than that during the digging phase.

The threshold of jet-flipping with respect to a range of tailwater depths and jet discharges rates was also investigated. Preliminary results on this aspect showed that for a particular apron length ratio and jet discharge, there is a critical tailwater whereby jet flipping will not occur if

its value is above the critical value and vice versa. Similarly for a particular apron length ratio and tailwater, there is a critical jet discharge such that jet flipping will occur if its value is higher than the critical value and vice versa.

ACKNOWLEDGEMENTS

The author would like to acknowledge and express his utmost gratitude to Dr. Lim Siow Yong, Project Supervisor, for his invaluable advice and professional guidance throughout the project who has made the completion of his project a success. The assistance of Ms. Xie Chen in the preparation of this report is highly appreciated. In addition, the author would also like to thank Mr. Lim Kok Hin, Mr. Foo Shiang Kim, Mr. Chia Key Huat, Mr. Fok Yew Seng and Mr. Syed Alwi Bin Sheikh Bin Hussien Alkaff for providing the necessary laboratory support and assistance while conducting the experiments.

TABLE OF CONTENTS

ABSTRACT.....	III
ACKNOWLEDGEMENTS	V
TABLE OF CONTENTS.....	VI
LIST OF TABLES	VIII
LIST OF FIGURES	IX
LIST OF SYMBOLS	XI
CHAPTER 1 INTRODUCTION	1
1.1 Purpose.....	1
1.2 Background	1
1.3 Scope of Study	2
1.4 Organization of the report	2
CHAPTER 2 LITERATURE REVIEW	3
2.1 Jet Flipping Phenomenon.....	3
2.1.1 Occurrence of Jet Flipping	3
2.2 Scour Downstream of a Sluice Gate	4
2.2.1 Velocity Profile in the Scour Region	4
2.2.2 Effect of Tailwater Depth.....	6
2.2.3 Effect of Apron Length	8
CHAPTER 3 EXPERIMENTAL SETUP AND PROCEDURES	9
3.1 Setup.....	9
3.2 Bed Sediment - Sieve Analysis	10

3.3	Procedures	13
CHAPTER 4 RESULTS AND DISCUSSIONS		15
4.1	General Observations and Characteristics on Scouring Process with Jet flipping	15
4.1.1	Typical Centreline Scour Profiles with Jet flipping	18
4.1.2	Time Scale of Dig and Fill Process	21
4.2	Effect of Apron Length on Time Scale	21
4.3	Maximum and Minimum Scour Depth	25
4.4	The Observation of Sand Ridge	29
4.4.1	Effect of Apron Length on Height of Ridge	33
4.5	Effect of Different Parameters on the Occurrence of Jet flipping.....	37
4.5.1	Effect of Tailwater Depth.....	37
4.5.2	Effect of Flowrate	38
CHAPTER 5 CONCLUSIONS.....		41
REFERENCES.....		43

LIST OF TABLES

Table 2.1 Experimental data and results (Dey and Westrich 2003).....	8
Table 3.1 Sand particle size analysis.....	12
Table 3.2 Unified Soil Classification System chart.....	13
Table 4.1 Summary of the experiments conducted for 2-D jets.....	17
Table 4.2 Summary of experimental data ($d_o = 10$ mm, $H_t = 12.7$ mm, $Q = 2.128$ L/s, $u_o = 0.71$ m/s, $Fr = 2.267$)	23
Table 4.3 Summary of data	40

LIST OF FIGURES

Figure 2.1 Magnitude of velocity vector in the x-z plane (Kurniawan and Altinakar 2002)	5
Figure 2.2 Schematic view of the flow field during (a) digging phase and (b) refilling phase (Balachandar and Kells 1997)	6
Figure 2.3 Effect of different tailwater depth on maximum scour depth versus F_o in the equilibrium state (Rajaratnam and Macdougall 1983)	7
Figure 2.4 Effect of different tailwater depth on location of maximum scour depth versus F_o in the equilibrium state (Rajaratnam and Macdougall 1983)	7
Figure 2.5 Scour hole profile for high submergence across the flume cross section (Deshpande, Balachandar et al. 2007)	7
Figure 3.1 Schematic Layout of Experimental Flume	9
Figure 3.2 Initial setting of sediment bed	10
Figure 3.3 Particle size distribution of sediment used	12
Figure 3.4 Definition sketch of digging process	14
Figure 3.5 Definition sketch of filling process	14
Figure 4.1 Jet impingement point and flow direction in digging phase	16
Figure 4.2 Water flow direction in filling phase	16
Figure 4.3 Shape of the centreline scour profiles for Run 21 during the first digging phase	19
Figure 4.4 Shape of the centreline scour profiles for Run 21 during the first filling phase	20
Figure 4.5 Time-sequence of each digging and filling phase for different apron lengths	22
Figure 4.6 Relationship of the ratio of the average digging to filling time, t_{fo}/t_{do} versus apron length ratio, L/d_o	24
Figure 4.7 Relationship between t_o , average time to complete one full dig-fill cycle and the apron length ratio, L/d_o	24
Figure 4.8 Relationship between ratio of scour depth (d_{st-dig}) to equilibrium scour depth ($d_{lse-dig}$)	

and ratio of digging duration for each cycle (t) to t_0 for Runs 20, 21, 22	26
Figure 4.9 Relationship between ratio of scour depth ($d_{st-fill}$) to equilibrium scour depth ($d_{lse-fill}$)	
and ratio of filling duration for each cycle (t) to t_0 for Runs 20, 21, 22	27
Figure 4.10 Effect of apron length ratio on maximum and minimum scour depth	28
Figure 4.11 Effect of apron length ratio on Δd_s	28
Figure 4.12 Development of sand ridge in the first 3 dig-fill cycles for Run 21	30
Figure 4.13 Development of sand ridge in the first 3 dig-fill cycles for Run 13	31
Figure 4.14 Run 13: Sequence of the current d_{h2} formation overtopping on d_{h1} formed from previous cycle	32
Figure 4.15 Run 13: Sequence of the current d_{h2} formation merging below d_{h1} formed from previous cycle	32
Figure 4.16 Relationship between ratio of ridge height (d_{h2}) to equilibrium ridge height (d_{1H-dig})	
and ratio of digging duration for each cycle (t) to t_0 for Runs 20, 21, 22	34
Figure 4.17 Relationship between ratio of ridge height (d_{h2}) to equilibrium ridge height ($d_{1H-fill}$)	
and ratio of filling duration for each cycle (t) to t_0 for Runs 20, 21, 22	35
Figure 4.18 Effect of apron length ratio on Δd_h	36
Figure 4.19 Time-sequence of each digging and filling phase for Run 79	38
Figure 4.20 Time-sequence of each digging and filling phase for Run 121	39

LIST OF SYMBOLS

d_h	=	height of ridge at any time
d_{h1}	=	height of ridge form from previous cycle or 1 st cycle
d_{h2}	=	height of ridge form in current cycle
d_{1H-dig}	=	height of ridge at equilibrium state during first digging phase
$d_{1H-fill}$	=	height of ridge at equilibrium state during first filling phase
d_s	=	depth of the movable plate below apron level
d_{se}	=	scour depth at equilibrium state
d_{se-dig}	=	maximum depth of scour at equilibrium state during each digging phase
$d_{se-fill}$	=	minimum depth of scour at equilibrium state during each filling phase
$d_{1se-dig}$	=	maximum depth of scour at equilibrium state during first digging phase
$d_{1se-fill}$	=	minimum depth of scour at equilibrium state during first filling phase
d_{st}	=	scour depth at any time
d_0	=	sluice gate opening or height of jet opening
d_i	=	grain diameter corresponding to i% finer
d_{50}	=	median grain diameter corresponding to 50% finer
σ_g	=	standard deviation of particle size distribution
g	=	acceleration due to gravity
L	=	length of rigid apron
μ	=	viscosity of water
ρ	=	density of water
S	=	specific gravity of sediment
ρ_s	=	density of sediment

H_t = tailwater depth

Q = Flowrate or Discharge

C_c = contraction coefficient

u_0 = mean jet velocity

Fr = Froude number

F_0 = Densimetric Froude number

L = length from apron edge

L_R = length from apron edge to peak of dune at equilibrium state

L_{se} = length from apron edge to section of maximum scour depth

L_m = length of the scour hole at equilibrium state

$\Delta d_s (\%)$ = % scour depth difference of d_{se-dig} and $d_{se-fill}$

$\Delta d_h (\%)$ = % ridge height difference of d_{IH-dig} and $d_{IH-fill}$

t = duration of scouring

t_0 = average time to complete one cycle of digging-filling phase

t_{d0} = average digging time

t_{f0} = average filling time

CHAPTER 1 INTRODUCTION

1.1 Purpose

This report is to write up on the past 1 year experimental study, analysis and database of the author's Final Year Project. The main objective is to observe and study the scouring characteristic downstream of a sluice gate with an apron which consists of two separate phases, digging and filling phase.

1.2 Background

Water jet discharge through hydraulic structure such as sluice gate will erode the unprotected channel bed downstream of the hydraulic structure. This is a common incident in hydraulic engineering. The water jet issuing from sluice gate has excessively high velocity hence high kinetic energy and capable of causing scour hole. The excessive erosion below unprotected outlet is one of the factors that lead to the instability or failure of the hydraulic structure.

In most of the cases, the digging phase will reach equilibrium after some period. However, under certain flow conditions, the equilibrium of digging phase may not be reached and the jet action will rapidly flip from bed to water surface. This is the commencement of filling phase. The switching of jet direction is called jet flipping phenomenon and these two phases will occur alternative to each other.

Scouring development for digging phase consists of three stages, an early stage with a rapid rate of scouring; a development stage with a slower rate of scouring; and late stage with a less observable scouring activity. At the late stage, a pseudo-equilibrium or asymptotic condition is attained, where the scour hole will retain its profile, and has no significant observable changes over time. On the other hand, the scour recovery for filling phase has a relatively stable rate of filling. However, the position of maximum scour depth move closer towards the hydraulic structure, hence it might pose a greater threat to the stability of the hydraulic structure.

The investigation of the changes and characteristics of scour development in the digging as well as filling phase is necessary. A series of experiments was carried out to find the effect of apron length on the scour development during the digging and filling phases for flow below a sluice gate and over an erodible bed.

1.3 Scope of Study

The objectives of the present work are:

1. To observe the development of the scouring process, and scouring characteristics with jet flipping caused by a two-dimensional horizontal jet discharging from a sluice gate.
2. To study the effect of apron length (L) and discharge (Q) in the formation of the scour hole and ridge height during the digging and filling phases.
3. To find out the effects of different parameters such as tailwater depth and flowrate on the occurrence of jet flipping.

1.4 Organization of the report

This report consists of 5 chapters. The first chapter is an introduction to the background of the present study. The second chapter discusses the relevant studies carried out in this field. In Chapter Three, the methodology of the experiments is introduced. Chapter Four focuses on the discussion and analysis of the experimental results. The last chapter is the conclusions of the present study.

CHAPTER 2 LITERATURE REVIEW

2.1 Jet Flipping Phenomenon

Generally the evolution of a scour can be divided into 4 phases, initial phase, development phase, stabilization phase and equilibrium phase (Hoffmans and Verheij 1997). There are other classifications of the scour phases with the same basic concept. However, some researchers found the equilibrium stage would never arrive under certain hydraulic conditions and a jet flipping phenomenon was observed during the scouring process (Johnston 1990; Balachandar and Kells 1997)

2.1.1 Occurrence of Jet Flipping

The tailwater ratio (H_t/d_o) or tailwater depth is the main parameter of jet flipping and some researchers have used jet flipping as the distinction between high and low submergence. Balachandar et al. (2000) and Bey et al. (2007) defined high jet submergence as a state where no flipping of the jet between the surface and bed was observed. Most of the researchers found that jet flipping only occurred at low submergence.

Ali and Lim (1986) studied the situation where the tailwater depth was between these two extremes. They showed that in large tailwater depth ($H_t/d_o > 10$), an asymptotic depth of scour was reached in a continuous manner. However, at smaller tailwater depth ($H_t/d_o < 5$), the data suggested that the scour hole did not undergo a continuous growth to the equilibrium stage. Johnston (1990) studied the plane jet emerged through a slot and the jet flipping was only observed under shallow submergence ($D/d_o = 2.33$ and 3.48 , D is defined as vertical distance from jet centre line of the slot to the free surface and d_o is the slot width).

In Balachandar and Kells (1997)'s work, 1 cm of apron length was applied downstream of the sluice gate, and the jet flipping only occurred under shallow jet submergence ($H_t/d_o = 6.5$). Deshpande, Balachandar and Mazurek (2007) confirmed the jet flipping phenomenon occurred in low submergence ($H_t/d_o = 4$) by measuring the velocity.

However, in the present study, jet flipping phenomenon was found under high submergence $H_t/d_o = 12.7$, which means the shallower submergence ratio was no longer the only reason to induce jet flipping. The occurrence of jet flipping might be related to the flow direction, jet exit velocity profile and the presence of apron length. The influence of flow direction and jet exit velocity profile will be further discussed in Section 2.2.1.

2.2 Scour Downstream of a Sluice Gate

Several researchers had studied the scouring process downstream of a sluice gate (Rajaratnam 1981; Rajaratnam and Macdougall 1983; Nik Hassan and Narayanan 1985; Ali and Lim 1986; Balachandar and Kells 1997; Karim and Ali 2000; Bey, Faruque et al. 2007; Deshpande, Balachandar et al. 2007; Dey and Sarkar 2007; Lim and Xie 2011). Dey and Sarkar (2006 & 2007) presented the scaling of time variation of scour depth by an exponential law and the effect of apron length, densimetric Froude number, sediment size, sluice opening as well as tailwater depth to the equilibrium scour depth.

Rajaratnam and MacDougall (1983) studied the erosion of sand bed by plane water wall jets with minimum tailwater depth and Deshpande, Balachandar and Mazurek (2007) had carried out the difference in scour profile due to 3 kind of strup conditions and the effect of high submergence to the local scour.

2.2.1 Velocity Profile in the Scour Region

The velocity profiles and distribution in the scour region were used by researchers to understand and explain the characteristics of the scouring and refilling process. Nik Hassan and Narayanan (1985) measured the mean velocity distributions after the scour reached equilibrium at the later stages and expressed the maximum velocity as a function of the distance along the apron:

$$\frac{U_m}{U_1} = 3.83 \left(\frac{X_L}{y_1} \right)^{-0.5} \quad (2.1)$$

where U_m = the maximum velocity

X_L = longitudinal distance from the sluice gate

y_1 = thickness of the jet at the vena contracta

U_1 = average velocity through vena contracta

They also expressed the rate of the scour with respect to time using a semi-empirical analysis as follows:

$$\frac{1}{(n+1)} \frac{dh}{dt} = \beta_1 \left[\frac{U_m^2}{g(s-1)h} \right]^n U_m \left[\frac{U_m^2}{g(s-1)D} \right] \quad (2.2)$$

h = maximum scour depth

β = a dimensionless coefficient

From the above equation, $n = 2$ gives the best shape of the curve of scour depth versus time.

Kurniawan and Altinakar (2002) measured the velocity distribution of the scour hole with (Fig 2.1 Exp C) and without (Fig 2.1 Exp B) apron by using Acoustic Doppler Velocity Profiler (ADVP). For Exp B, without apron, the measurement shows that the flow issued from the sluice gate impinges on the bed. In present study, this is called bed jet and it occurs in digging phase. When apron is applied (Exp C), the jet is deflected towards surface instead of impinging to the bed, this is named as surface jet in present study and it occurs in filling phase.

The results were in a good agreement with Balachandar and Kells (1997) which observed the flow pattern by dye injection (Fig 2.2). From Fig 2.1 and 2.2, two recirculation regions are observed in both phases.

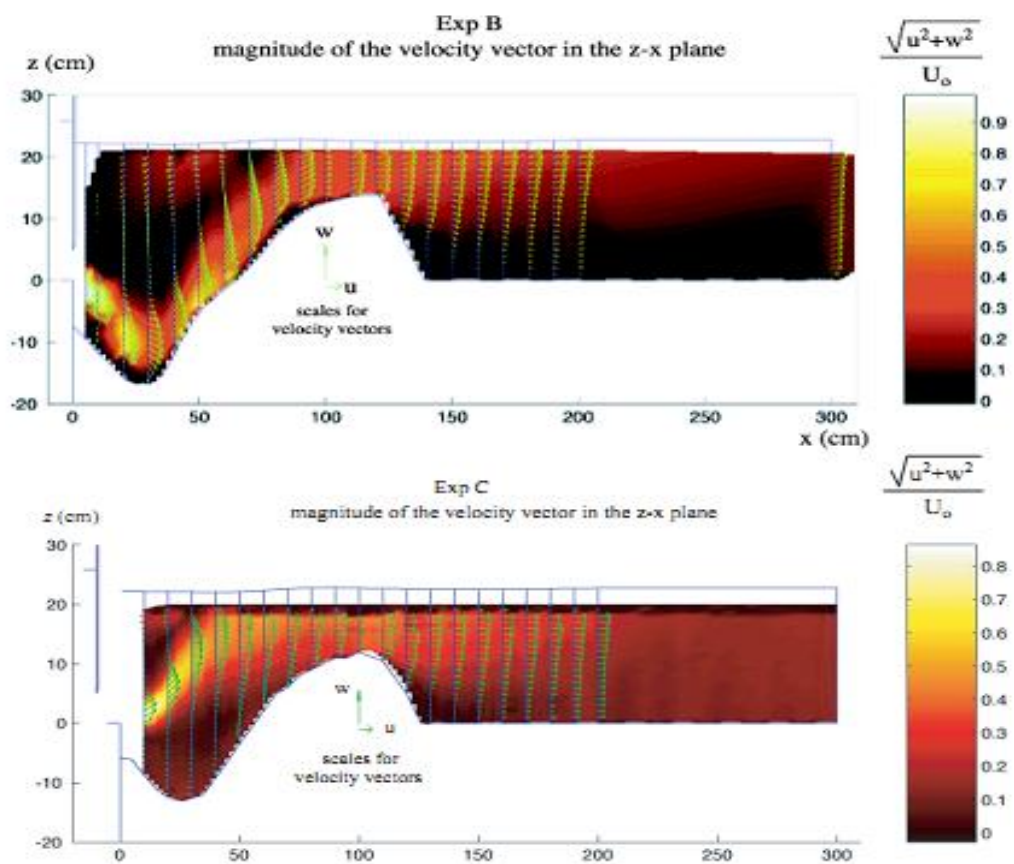


Figure 2.1 Magnitude of velocity vector in the x-z plane (Kurniawan and Altinakar 2002)

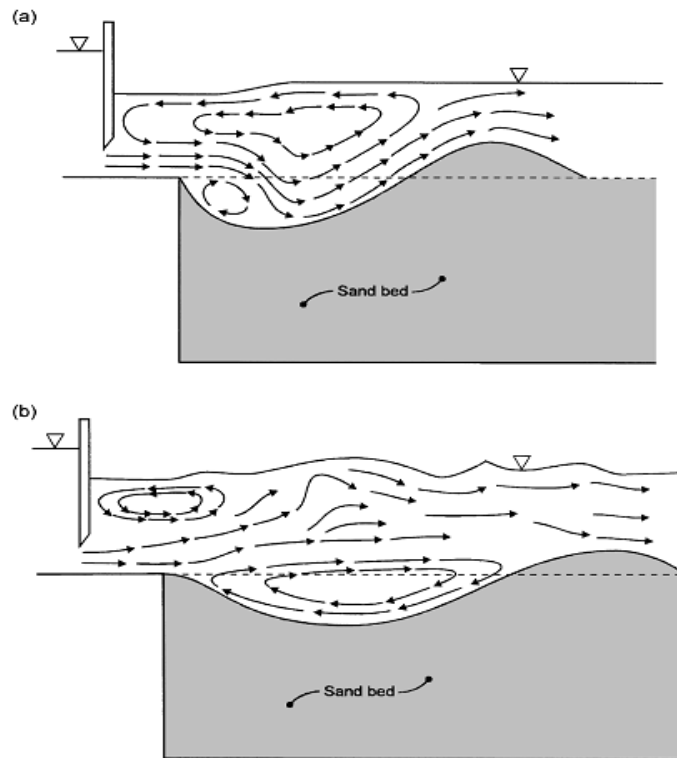


Figure 2.2 Schematic view of the flow field during (a) digging phase and (b) refilling phase (Balachandar and Kells 1997)

2.2.2 Effect of Tailwater Depth

The tailwater depth, H_t is an important parameter in the scour depth during equilibrium or pseudo equilibrium stages. Generally, the equilibrium scour depth increases with decreases in tailwater depth.

However, under shallow tailwater conditions, the process of scour development is more complex compared to relatively deep tailwater conditions. Ali and Lim (1986) studied the scour due to two and three-dimensional submerged wall jets in shallow tailwater conditions. They found that there was a critical tailwater depth, beyond which scour depth tends to increase irrespective of the increase of tailwater depth.

Rajaratnam and Macdougall (1983) considered the erosion of sand beds by plane turbulent water wall jets when the tailwater depth was approximately equal to the jet thickness. The results of the experiment showed the maximum depth of erosion were smaller than usual cases where the tailwater depth was larger (Figure 2.3). From Figure 2.4, it indicates the maximum scour section is located further downstream from the gate. In this case, there was no formation of sand ridge downstream of the scour hole, all the suspended material was transported by the flow out of the test section of the flume.

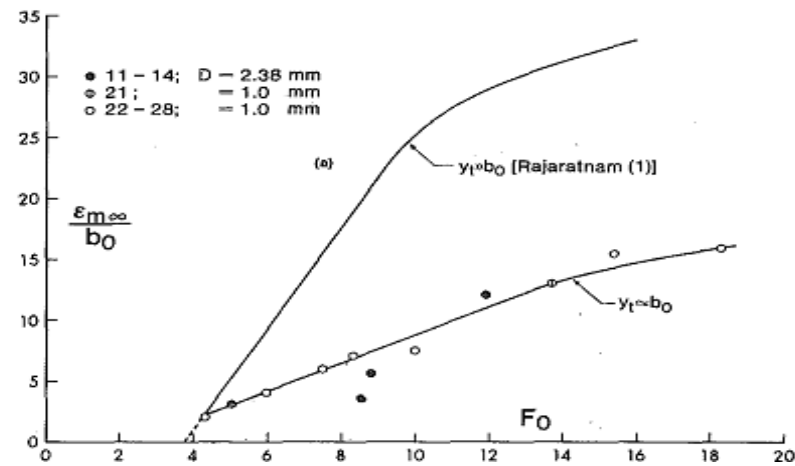


Figure 2.3 Effect of different tailwater depth on maximum scour depth versus F_o in the equilibrium state (Rajaratnam and Macdougall 1983)

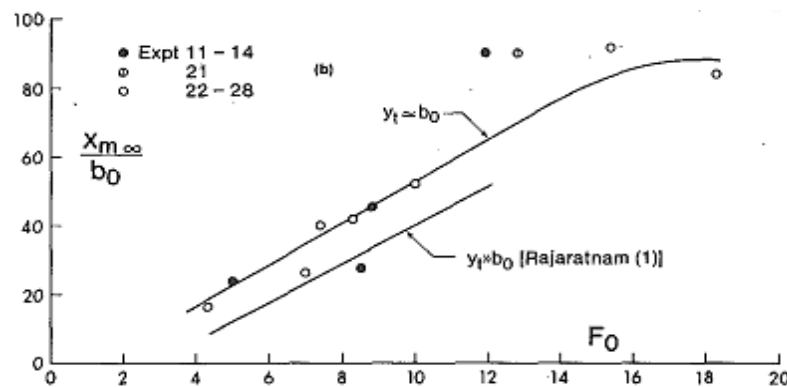


Figure 2.4 Effect of different tailwater depth on location of maximum scour depth versus F_o in the equilibrium state (Rajaratnam and Macdougall 1983)

Deshpande, Balachandar and Mazurek (2007) studied the effect of submergence to the scour. Figure 2.5 shows the centreline scour profiles for three tailwater depths ($y_t/b_o = 8, 12, 20$). The profiles for two larger tailwater ratio ($y_t/b_o = 12, 20$) are similar. However, for smaller tailwater ratio ($y_t/b_o = 8$), scour depth increase with decreasing submergence.

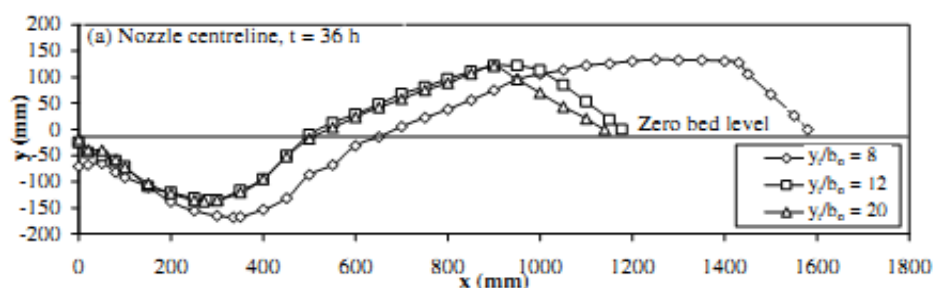


Figure 2.5 Scour hole profile for high submergence across the flume cross section (Deshpande, Balachandar et al. 2007)

2.2.3 Effect of Apron Length

Dey and Westrich (2003) had studied the scouring of a cohesive bed downstream of an apron due to a submerged horizontal jet issuing from a sluice opening. They had used a relatively longer apron length (> 0.30 m) to conduct the experiment. In Table 2.1, the experiments have done in different set of parameters and the result of scour depth is shown.

Table 2.1 Experimental data and results (Dey and Westrich 2003)

Run number	L (m)	b_o (m)	U_o (m/s)	h (m)	Δh (m)	d_s (mm)							
						$t=1$ min	5 min	10 min	15 min	30 min	60 min	120 min	180 min
1	0.60	0.02	1.398	0.126	0.125	5.0	13.0	19.0	24.0	31.0	39.0	45.0	51.0
2	0.45	0.02	1.398	0.127	0.123	5.5	15.0	19.5	26.0	35.0	43.0	50.0	55.0
3	0.45	0.02	0.968	0.124	0.056	4.0	7.5	14.0	19.0	24.0	30.0	34.0	37.5
4	0.45	0.03	0.935	0.132	0.044	4.5	11.0	16.0	20.0	26.0	32.0	36.0	41.0
5	0.45	0.03	0.645	0.121	0.024	3.0	8.0	12.0	16.0	21.0	26.0	31.0	35.0
6	0.45	0.04	0.699	0.127	0.032	3.5	7.0	10.0	13.0	17.0	22.0	26.0	29.0
7	0.30	0.02	1.398	0.132	0.113	9.0	18.0	32.0	37.0	51.0	64.0	75.0	80.0
8	0.30	0.02	0.968	0.125	0.052	5.0	11.0	18.0	22.0	28.0	35.5	42.0	45.0
9	0.30	0.03	0.935	0.130	0.046	6.0	14.0	20.0	25.0	32.0	40.0	45.0	51.0
10	0.30	0.03	0.645	0.122	0.026	4.5	10.5	17.0	21.0	27.0	33.0	37.5	42.0
11	0.30	0.04	0.699	0.128	0.032	5.0	12.0	18.0	22.0	29.0	35.6	41.5	46.0
12	0.30	0.04	0.484	0.120	0.017	3.0	7.0	10.0	13.0	17.0	21.0	24.0	26.0

The effect of apron length can be seen by comparing a few sets of data in Table 2.1, for example, Run 1, 2 and 7, Run 3 and 8, Run 4 and 9, Run 5 and 10. These sets of data show that deeper scour depths have been observed by decreasing apron length.

In Dey and Sarkar (2006)'s work, again, their conclusion was the equilibrium scour depth increased with decreased in apron length. Besides, they had studied the reduction of scour depth by placing a launching apron downstream of the rigid apron, and the results showed that the reduction could reach a maximum of 57.3%.

CHAPTER 3 EXPERIMENTAL SETUP AND PROCEDURES

3.1 Setup

Experiments were performed in the Hydraulics Laboratory at Nanyang Technological University. A deep glass-wall flume of length 8m, width 0.3m, and height 0.6m (Figure 3.1) with a recirculation arrangement of water was used for the experimentation. The glass-wall on both sides was provided for visual observations. A solid platform was mounted to simulate a rigid apron over which a vertical sharp edge sluice gate was installed. The sluice gate can be slide to any location along the apron, and the opening size can be changed. This arrangement facilitates the study of the effect of apron length on scouring characteristic downstream of a sluice gate. The length of apron (L) is measured from the right edge of apron to the tip of the vertical sharp edge sluice gate.

In sediment bed (Figure 3.2), uniform green sand with median grain diameter (d_{50}) of 0.73 mm was used and the geometric standard deviation (σ_g) was 1.12. The sand bed was 20.6 cm thick and was heightened with the rigid apron.

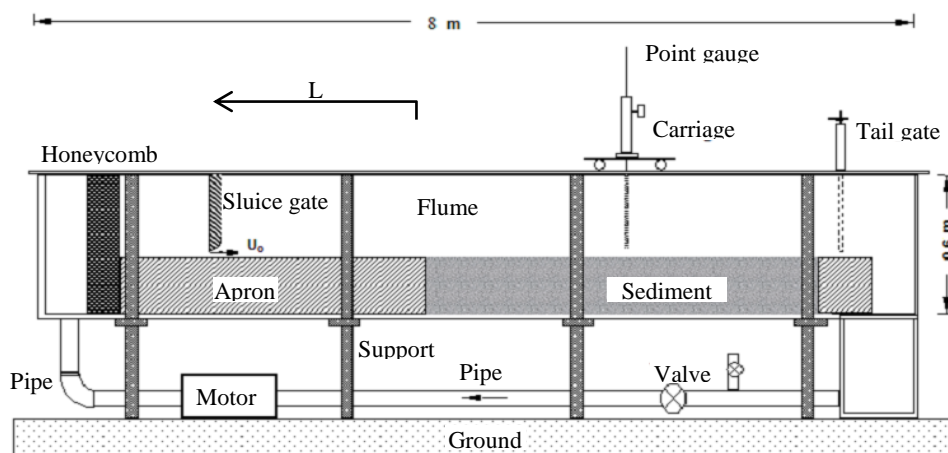


Figure 3.1 Schematic Layout of Experimental Flume

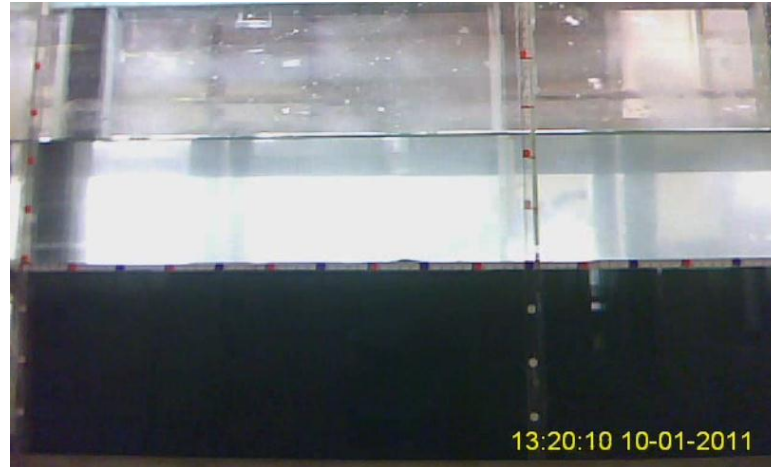


Figure 3.2 Initial setting of sediment bed

Water was pumped from the water storage tank into the inlet of flume by a series of pipes. The pipes were arranged in a honeycomb to reduce the turbulence of the incoming flow. The sand bed was connected with a sediment box to retain or trap the sand. The flow from the outlet or tailgate of the flumes was collected by a storage tank for recirculation within the flow circuit.

A high resolution webcam connected to a computer was used to record the scouring process continuously for a long period of time. Video software was used to automatically save the recorded video images every hour. This set up require less storage volume and good for long duration record of the scouring process. The video recording used up to 2 GB data storage per day and it allowed the long period experiments to be viewed subsequently. Most importantly, this set up allowed the author to observe whether jet flipping occurred during the scouring process and decided the duration of the experiments.

3.2 Bed Sediment - Sieve Analysis

Soil materials from the sediment bed, maybe classified as: non-cohesive sediments and cohesive sediments. As the term implies, non-cohesive sediments are those consisting of discrete particles, the movement due to a given erosion forces, depends only on particle properties, e.g. shape, size, density, and the relative position of the particle with respect to surrounding particles. The present study will focus on the non-cohesive sediment and the same soil material is used for all the experiments.

Unified Soil Classification System (USCS) is used to quantify the percentage of distribution of different grain sizes. Grain size distribution, also known as gradation, is widely used for soil classification systems. It is a plot of the distribution of various grain sizes in a soil sample against the function of the percentage by weight passing a given sieve size. Gradation are

determined by sieve analysis, where soil sample is dried in oven and poured into a series of sieves stacked in descending sieve opening size. The sieves are then vibrating using a mechanical shaker and the retention soil on each sieve is weighed. Table 3.1 and Figure 3.3 show the result of sieve analysis of the soil material used in sediment bed.

The standard deviation of the grain size distribution, σ_g , is estimated using:

$$\sigma_g = \sqrt{\frac{d_{84}}{d_{16}}} \quad (3.1)$$

where d_{84} and d_{16} are the grain diameter in 84% and 16% passing respectively

The sediment will be categorized as uniform when $\sigma_g < 1.5$, and non-uniform when $\sigma_g \geq 1.5$. From Figure 3.3, the mean sediment size $d_{50} = 0.73$ mm, $d_{84} = 0.82$ mm and $d_{16} = 0.65$ mm. Thus, $\sigma_g = 1.12$ for the soil used and it can be classified as uniform. The specific gravity of the sand is 2.65.

Coefficient of uniformity, C_u and coefficient of curvature, C_c are the two parameters used in Unified Soil Classification System (USCS) to determine the soil gradation, i.e. well or poorly graded, high or low plasticity. Eq. 3.2 and 3.3 represent the equation for coefficient of uniformity, C_u and coefficient of curvature, C_c

$$C_u = \frac{d_{60}}{d_{10}} \quad (3.2)$$

$$C_c = \frac{d_{30}^2}{d_{60} \times d_{10}} \quad (3.3)$$

where d_{10} , d_{30} and d_{60} are the grain diameter in 10%, 30% and 60% passing respectively

From Figure 3.3, d_{10} , d_{30} and d_{60} are 0.61 mm, 0.70 mm and 0.78 mm. Thus $C_u = 1.28$ and $C_c = 1.03$. From Table 3.2, the sand used in bed sediment is poorly graded sand (mark in red circle).

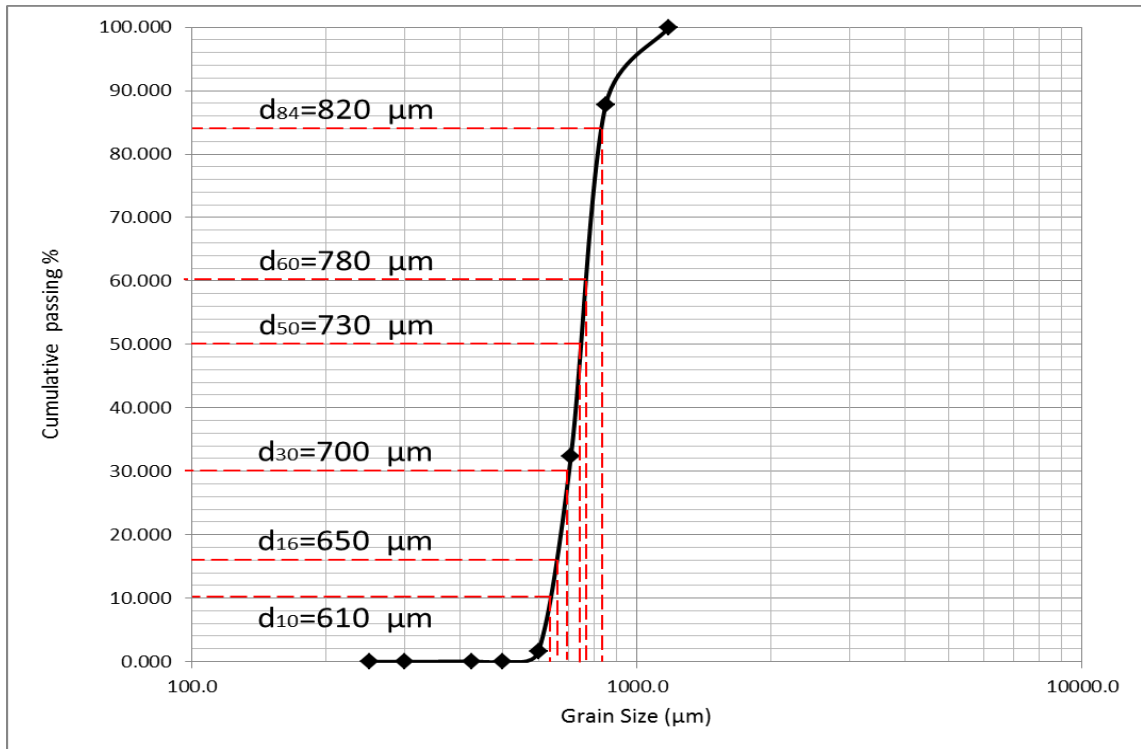


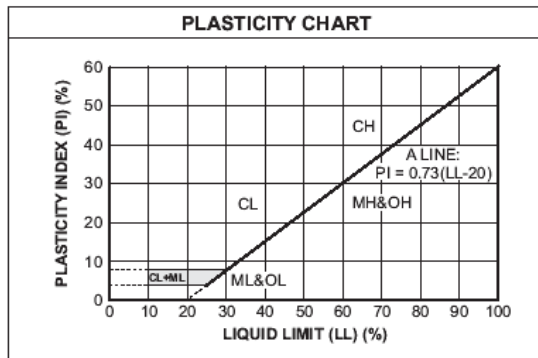
Figure 3.3 Particle size distribution of sediment used

Table 3.1 Sand particle size analysis

Sieve size (μm)	Mass of sieve (g)	Mass of sieve & sediments (g)	Mass Retained (g)	Retained %	Cumulative Retained %	Finer %
1180.0	401.200	401.200	0.000	0.000	0.000	100.000
850.0	355.700	414.800	59.100	12.256	12.256	87.744
710.0	351.500	618.600	267.100	55.392	67.648	32.352
600.0	348.200	496.600	148.400	30.776	98.424	1.576
500.0	342.000	349.400	7.400	1.535	99.959	0.041
425.0	326.400	326.500	0.100	0.021	99.979	0.021
300.0	313.400	313.500	0.100	0.021	100.000	0.000
250.0	304.400	304.400	0.000	0.000	100.000	0.000
Pan	0.0	0.0	0.0	0.0		
Sum			482.2			

Table 3.2 Unified Soil Classification System chart

UNIFIED SOIL CLASSIFICATION AND SYMBOL CHART			LABORATORY CLASSIFICATION CRITERIA	
COARSE-GRAINED SOILS (more than 50% of material is larger than No. 200 sieve size.)				
GRAVELS More than 50% of coarse fraction larger than No. 4 sieve size	Clean Gravels (Less than 5% fines)		$C_u = \frac{D_{60}}{D_{10}}$ greater than 4; $C_c = \frac{D_{30}}{D_{10} \times D_{60}}$ between 1 and 3	
	GW	Well-graded gravels, gravel-sand mixtures, little or no fines	GP Not meeting all gradation requirements for GW	
	GP	Poorly-graded gravels, gravel-sand mixtures, little or no fines		
	Gravels with fines (More than 12% fines)		GM Atterberg limits below "A" line or P.I. less than 4 GC Atterberg limits above "A" line with P.I. greater than 7	
	GM	Silty gravels, gravel-sand-silt mixtures		
	GC	Clayey gravels, gravel-sand-clay mixtures	Above "A" line with P.I. between 4 and 7 are borderline cases requiring use of dual symbols	
SANDS 50% or more of coarse fraction smaller than No. 4 sieve size	Clean Sands (Less than 5% fines)		$C_u = \frac{D_{60}}{D_{10}}$ greater than 4; $C_c = \frac{D_{30}}{D_{10} \times D_{60}}$ between 1 and 3	
	SW	Well-graded sands, gravelly sands, little or no fines	SP Not meeting all gradation requirements for GW	
	SP	Poorly graded sands, gravelly sands, little or no fines		
	Sands with fines (More than 12% fines)		SM Atterberg limits below "A" line or P.I. less than 4 SC Atterberg limits above "A" line with P.I. greater than 7	
	SM	Silty sands, sand-silt mixtures		
	SC	Clayey sands, sand-clay mixtures	Limits plotting in shaded zone with P.I. between 4 and 7 are borderline cases requiring use of dual symbols.	
FINE-GRAINED SOILS (50% or more of material is smaller than No. 200 sieve size.)				
SILTS AND CLAYS Liquid limit less than 50%	ML	Inorganic silts and very fine sands, rock flour, silty of clayey fine sands or clayey silts with slight plasticity	Determine percentages of sand and gravel from grain-size curve. Depending on percentage of fines (fraction smaller than No. 200 sieve size), coarse-grained soils are classified as follows: Less than 5 percent GW, GP, SW, SP More than 12 percent GM, GC, SM, SC 5 to 12 percent Borderline cases requiring dual symbols	
	CL	Inorganic clays of low to medium plasticity, gravelly clays, sandy clays, silty clays, lean clays		
	OL	Organic silts and organic silty clays of low plasticity		
SILTS AND CLAYS Liquid limit 50% or greater	MH	Inorganic silts, micaceous or diatomaceous fine sandy or silty soils, elastic silts		
	CH	Inorganic clays of high plasticity, fat clays		
	OH	Organic clays of medium to high plasticity, organic silts		
HIGHLY ORGANIC SOILS	PT	Peat and other highly organic soils		



3.3 Procedures

First, adjust the tailwater depth to a determined level. Then, switch off the pump in order to flatten the sand bed profile. Before activate the pump, cover the sand bed profile with a metal plate to prevent the bed from being disturbed by the jet when tailwater depth is under the required depth. After that, turn on the pump and wait the tailwater depth reaches to the required height. At the same time, start the webcam to record the flow and scouring action. Once the tailwater depth reaches the required height, remove the plate gently to reduce the disturbance of metal plate to the sand bed. The sediments or sand particles start to move and a scour hole is formed immediately downstream of the gate. Normally digging phase is observed at the initial of the experiments. The development of the scour is recorded by the webcam, and a stop-watch is used to record the scouring duration as a back-up. The scour profile changes with respect to

time and the hole could be observed to lengthen and deepen during the digging phase. Scour profiles at different time are plotted on the glass-wall as a back-up.

Generally, the scouring or digging rate is rapid at the initial period. Then the scouring rate slows down after a certain time and reaches to a pseudo equilibrium state. The duration to reach the pseudo equilibrium state is dependent on the hydraulics conditions. In some cases, a filling phase will take over the digging phase (jet flipping occur) and the sand is filled back at a steady rate, this is a cyclical process when jet flipping occurs. Normally, experiments associated with jet flipping will run for 2 to 4 weeks, but for some cases, a 7 or 10 days period is enough for the experiments to reach the equilibrium state.

Figures 3.4 and 3.5 show a definition sketch of the digging and filling process. In Chapter 4, the definition of symbols in analysis and discussion will be based on these two sketches.

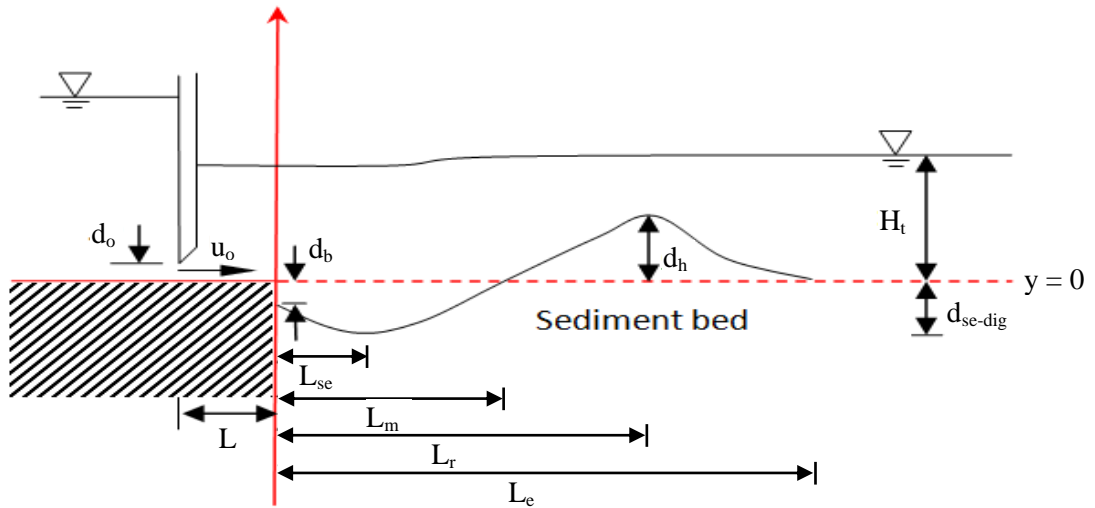


Figure 3.4 Definition sketch of digging process

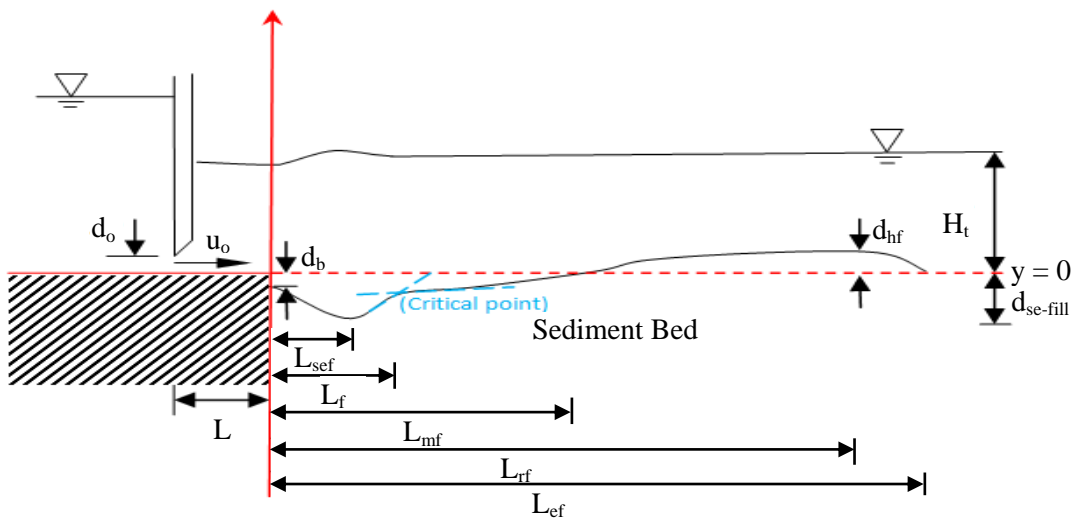


Figure 3.5 Definition sketch of filling process

CHAPTER 4 RESULTS AND DISCUSSIONS

4.1 General Observations and Characteristics on Scouring Process with Jet flipping

Under certain flow conditions (see Table 4.1) there would be jet flipping, where the scouring process might not reach an equilibrium and water jet suddenly flipped from the bed to surface (Lim and Xie 2011; Ling 2011). During digging process, the direction of discharged water jet was unstable (Lim and Chiew 2001). The jet impingement point was oscillating in horizontal direction along the scour hole and the mean location of impingement was close to maximum scour depth (Bey, Faruque et al. 2007). Figure 4.1 shows the jet impingement point and flow direction after contact with the scour hole in the digging phase. Blue dye was used to indicate the water jet streamline. In Figure 4.1(a), concentrated blue dye is observed in the opening of sluice gate, followed by Figure 4.1(b) which shows the blue dye reaching the location of maximum scour depth. Then, the water jet spreads into two directions, a portion of water flow back to the direction of sluice gate opening and formed a recirculation region. This recirculation streamline is shown as yellow line in Figure 4.1(c). Another portion of water flow along downstream of the maximum scour depth and is indicated as red line in Figure 4.1(c). This portion of flow later will divide into two parts; the purple line in Figure 4.1(d) shows the portion of water that flows over the sand ridge and continues to the downstream of the sand ridge. The formation of sand ridge downstream of the scour hole was mainly caused by the accumulation of sand particles that were transported by this flow. The dark blue line in Figure 4.1(d) shows the water that flow back to the upper part of sluice gate and form another recirculation region. Therefore, at the digging process, two recirculation regions were formed and this observation is quite similar to the results of velocity measurements by Kurniawan and Altinakar (2002).

Throughout the entire process, the water jet is attached to the bed after releases from the sluice gate opening; this is defined as the bed jet. During the digging phase, water surface is very clam (see Figure 4.1).

After some period of continuous digging, the scour reached a pseudo-equilibrium state and the bed profile had no significant changes in geometry. At this stage, the bed jet suddenly would flip upwards and transformed into a surface jet and the water surface started to become very choppy. This was the indication of the commencement of the filling phase. During the filling process, the sand particles in sand ridge were filled back to the scour hole. The water flow

direction is shown in Figure 4.2. From Figure 4.2 (a), water jet that eject from the sluice gate flow to the water surface directly. After that, the water jet spreads into two directions, a small part of water flowed back to the upper part of sluice gate and formed a recirculation region. The other part of water flowed to the direction of sand ridge. Then, when the water flowed further downstream, it splits into two portions before it reached the maximum ridge height. The first portion of water flowed downward along the sand bed and ‘dragged’ the sand particles on the sand ridge back to the scour hole. This formed the second recirculation region in the filling phase. On the other hand, the second portion of water continued to flow over the sand ridge. In preliminary conclusion, there are two recirculation regions found in both phases, where the second recirculation region in filling phase is very important as it participates in the deposition of sand particles back to the scour hole.

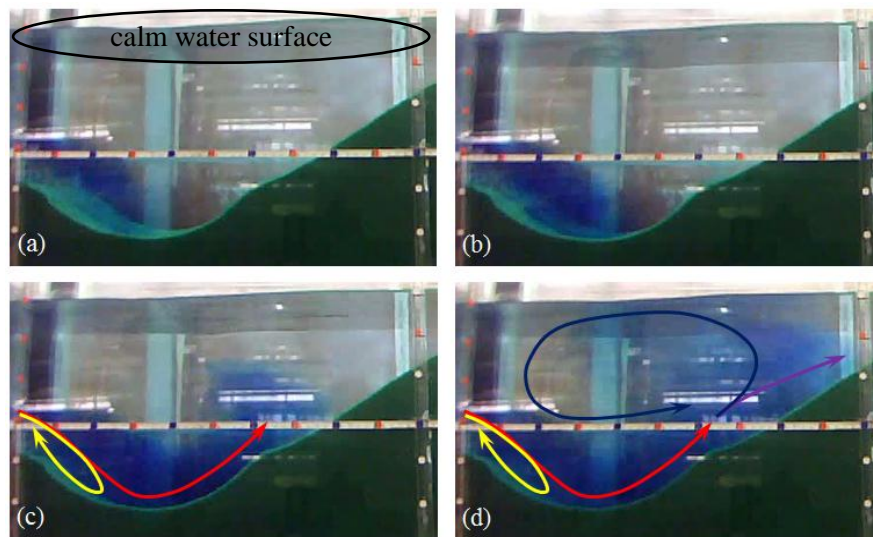


Figure 4.1 Jet impingement point and flow direction in digging phase

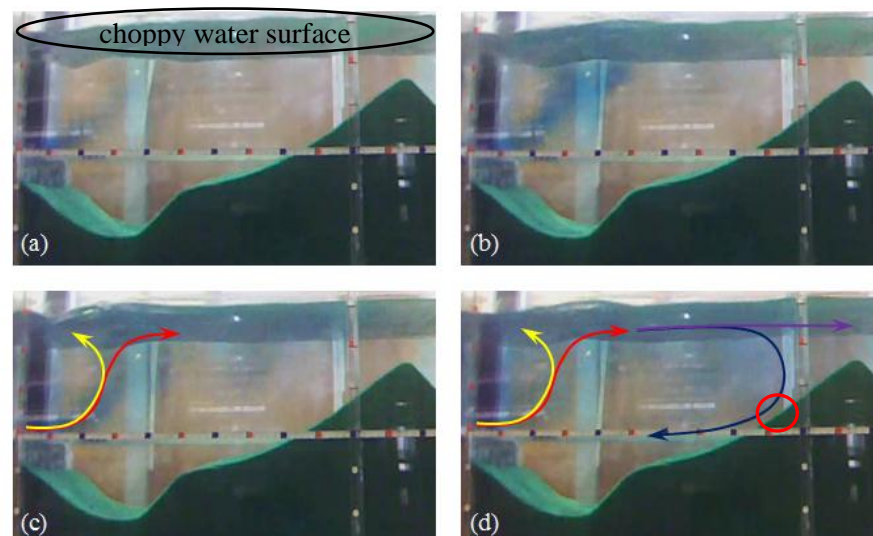


Figure 4.2 Water flow direction in filling phase

Table 4.1 Summary of the experiments conducted for 2-D jets

Run	t_o (min)	L(mm)	Q (L/s)	H_i (cm)	U_o (m/s)	d_{se-dig} (cm)	$d_{se-fill}$ (cm)	Δd_s (%)	d_{se-dig}/d_o	H_i/d_o	F_o	No. of flipping cycles / scour duration
13	257	210	2.128	12.7	0.71	6.5	4.6	29	6.5	12.7	6.53	41 for 7 days
14	23	300	2.128	12.7	0.71	3.9	2.8	28	3.9	12.7	6.53	70 for 2 days
15	936	150	2.128	12.7	0.71	8.1	5.1	37	8.1	12.7	6.53	9 for 7 days
17	44	210	3.33	11	1.11	7.2	2.8	61	7.2	11	10.21	62 for 3 days
18	31	210	2.5	12.7	0.83	4.4	2.4	45	4.4	12.7	7.67	90 for 3 days
19	1225	150	2.083	12.7	0.69	8.8	6	32	8.8	12.7	6.53	15 for 13 days
20	1097	90	2.128	12.7	0.71	9.6	5.2	46	5.2	12.7	6.53	8 for 7 days
21	2349	30	2.128	12.7	0.71	12	8	33	12	12.7	6.53	12 for 22 days
22	1149	10	2.128	12.7	0.71	13.8	10.4	25	1.4	12.7	6.53	23 for 18 days
52	27	300	2.128	16	0.709	4.38	3.02	31	4.38	16	6.526	207 for 4 days
79	3524	90	1.818	12.7	0.606	8.47	7.1	16	8.47	12.7	5.575	11 for 28days
81	119	210	1.818	12.7	0.606	3.99	3.31	17	3.99	12.7	5.575	48 for 4 days
82	52	300	1.818	12.7	0.606	2.95	2.33	21	2.95	12.7	5.575	10 for 1 day
121	1158	90	2.5	16	0.833	13.6	7.9	42	13.6	16	7.666	12 for 12 days
122	1839	150	2.5	16	0.833	9.17	7.9	14	9.17	16	7.666	12 for 18 days

4.1.1 Typical Centreline Scour Profiles with Jet flipping

Figures 4.3 and 4.4 show the typical shape of the centreline bed profiles during scouring process for a complete jet flipping cycle in Run 21 (1st Cycle). The profiles in Figure 4.3 constitute the digging phase by the attached bed jet and the total duration is around 253,000 seconds. The digging started with yellow lines; the duration of yellow lines was 100 seconds. Then the profile developed into green lines which had a total duration of the 900 seconds. In Run 21, the first 1,000 seconds had a rapid scouring rate which sees half of the total digging process completed with respect to its scour depth and scour width. After that, the profiles in blue lines correspond to the next 9,000 seconds and pink lines represent the profiles in the next 90,000 seconds. These two set of lines showed a lower scouring rate but the scouring process is still on going. Lastly, the late stage profiles were plotted in red lines with a total duration of 153,000 seconds. During this stage, only a few scouring activity was observed and a pseudo equilibrium state was reached.

After the last profile in Figure 4.3, the video recording showed that the jet suddenly flips towards the water surface and the filling phase begins. The surface jet caused the sand particles on sand ridge to roll down its slope and filled the scour hole. In Figure 4.4, the profiles from yellow to green, then blue and lastly pink gave the shapes of the scour hole during the filling process. It was noted that the height of ridge would increase at the initial stage before it decreased. This interesting observation will be explained in Section 4.4.1.

Duration of first filling process in Run 21 consumed about 36,000 seconds. At the end of filling phase, the ridge height was lower and the minimum scour depth was much shallower compare with the initial profile. In Run 21, the duration to reach a pseudo equilibrium stage for the filling phase is much shorter than the digging phase. The occurrence of digging and filling process was cyclical and many cycles had been documented over the recording period (see Table 4.1).

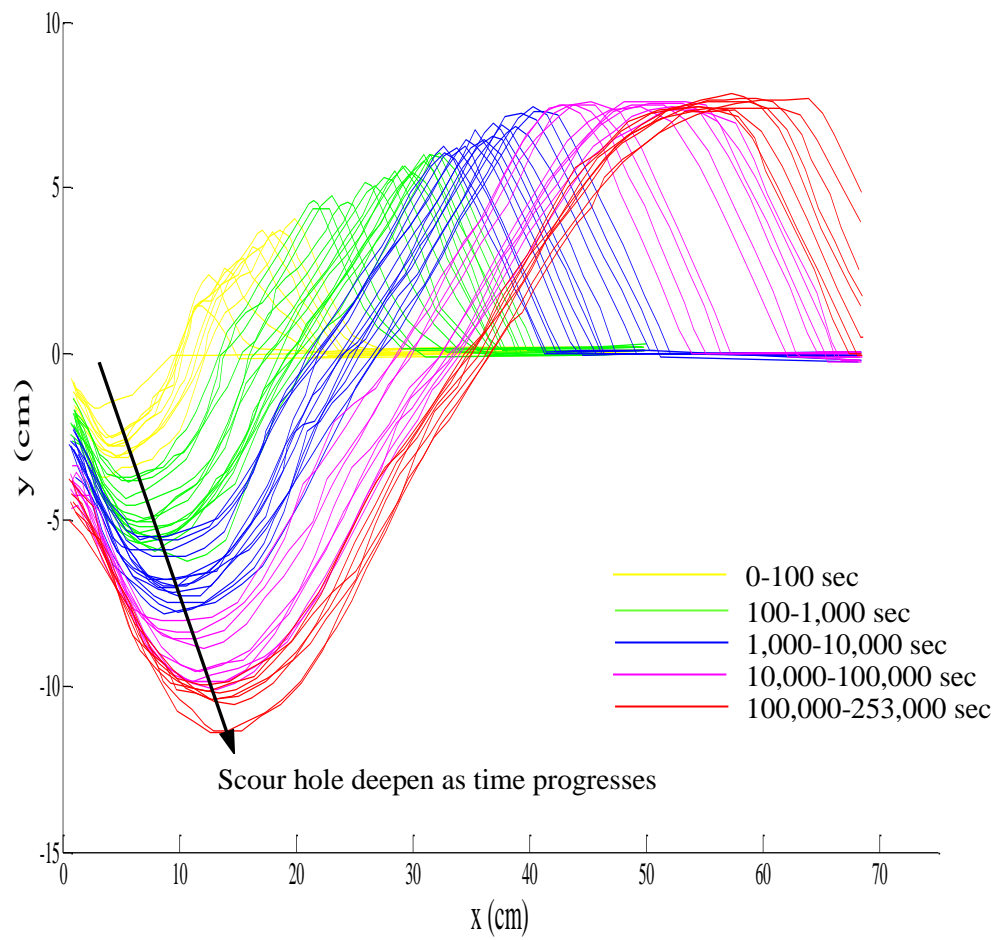


Figure 4.3 Shape of the centreline scour profiles for Run 21 during the first digging phase

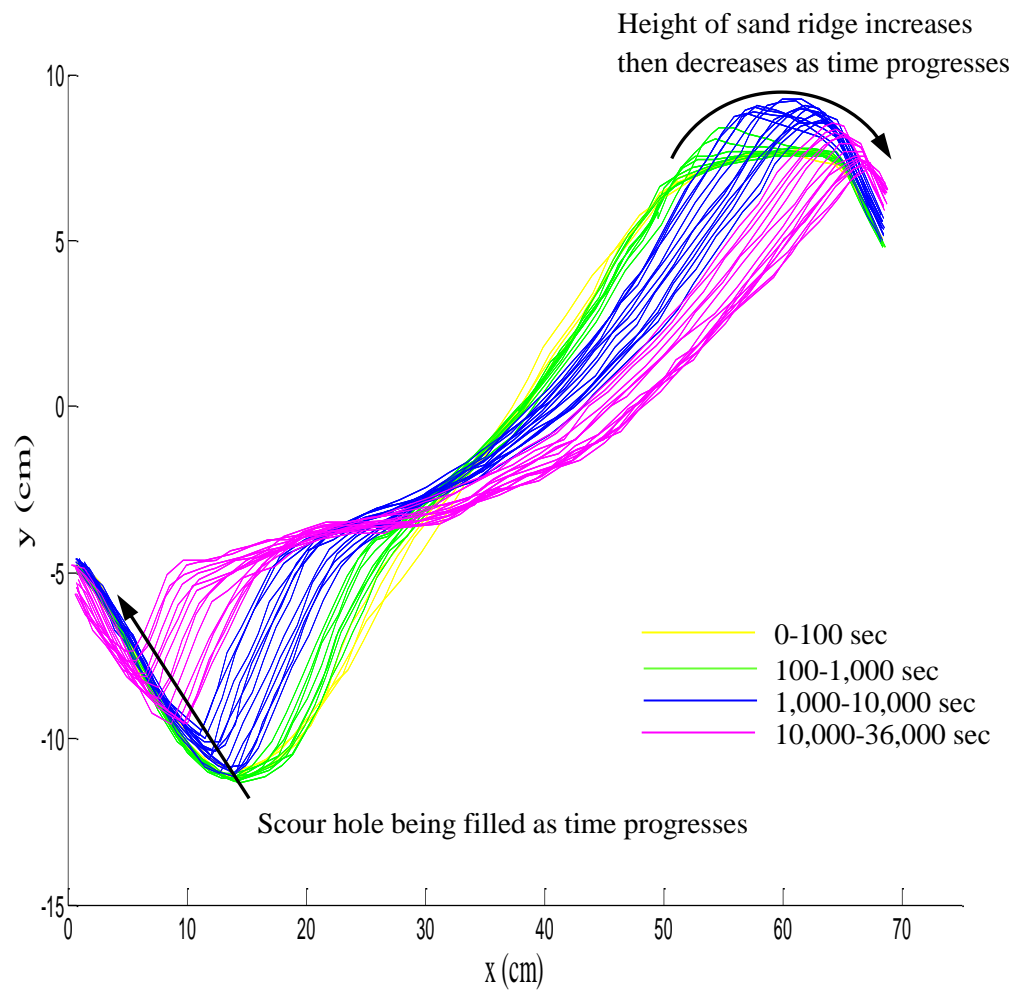


Figure 4.4 Shape of the centreline scour profiles for Run 21 during the first filling phase

4.1.2 Time Scale of Dig and Fill Process

In Table 4.1, a time scale, t_o which is the average time to complete one dig-fill cycle of digging and filling phase (Lim and Xie 2011), i.e. the time from the start of filling phase in i^{th} cycle to the end of digging phase in $(i+1)^{\text{th}}$ cycle is proposed,

$$t_o = \frac{\sum_{i=1}^{n-1} (t_{f_i} + t_{d_{i+1}})}{n-1} \quad (4.1)$$

where n is the total number of digging-filling cycles recorded for an experiment or Run, t_{f_i} and $t_{d_{i+1}}$ are the duration of filling phase in the i^{th} cycle and duration of digging phase in the $(i+1)^{\text{th}}$ cycle, respectively.

From the above equation, the duration of the digging phase in the first cycle is ignored in determining t_o . For most of the experiments that have jet flipping, it was observed that the period recorded for the digging time in the first cycle was much longer than the digging time of subsequent cycles. This is shown in the Figure 4.5, the digging time of first cycle are marked in circle. This difference in digging time can be explained as the scouring action for first digging begins from an original flatbed condition while the subsequent cycles start from the minimum scour depth, $d_{\text{se-fill}}$ from the previous cycles' filling phase. Therefore, extra time may be required for the first digging phase to dig to the maximum scour depth at equilibrium state during the first digging phase, $d_{\text{lse-dig}}$. As a result, the first digging time may be ignored when calculating the t_o .

In addition, the average digging time, t_{d0} and filling time, t_{f0} can be defined as follow,

$$t_{d0} = \frac{\sum_{i=1}^{n-1} (t_{d_{i+1}})}{n-1} \quad (4.2)$$

$$t_{f0} = \frac{\sum_{i=1}^{n-1} (t_{f_i})}{n-1} \quad (4.3)$$

And the relationship between t_o , t_{d0} and t_{f0} can be expressed as,

$$t_o = t_{d0} + t_{f0} \quad (4.4)$$

4.2 Effect of Apron Length on Time Scale

Runs 13, 14, 15, 16, 20, 21, 22, 161 and 162 were conducted with the same tailwater depth ($H_t = 12.7$ cm), sluice gate opening ($d_o = 10$ mm), discharge ($Q = 2.128$ L/s), velocity ($u_o = 0.71$ m/s), Froude number ($Fr = 2.267$) but different apron length (L) (Table 4.2). Figure 4.5 shows the total duration of each digging and filling phase along with the number of cycles for Runs that have jet flipping.

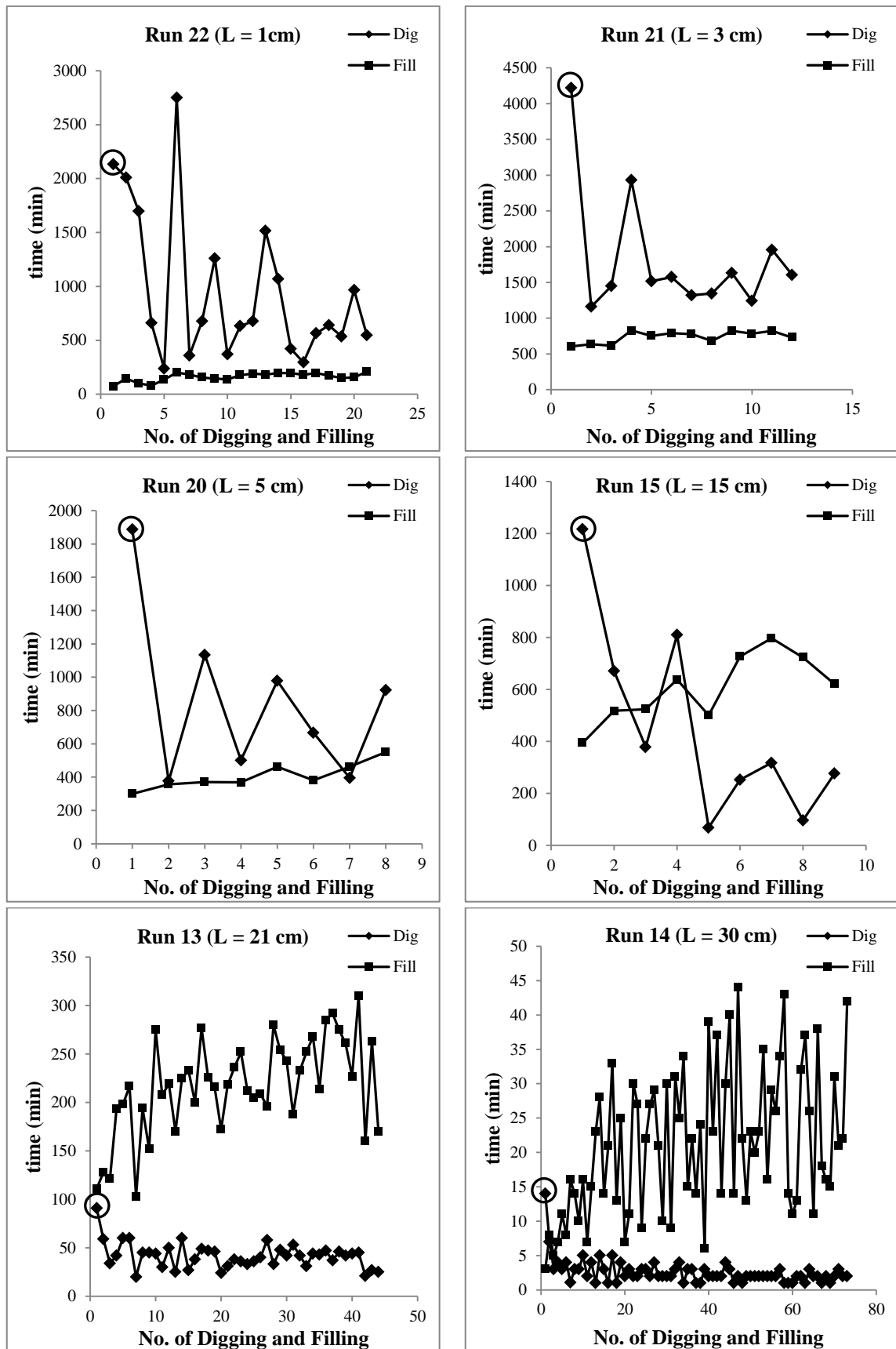


Figure 4.5 Time-sequence of each digging and filling phase for different apron lengths

Table 4.2 Summary of experimental data ($d_o = 10$ mm, $H_t = 12.7$ mm, $Q = 2.128$ L/s, $u_o = 0.71$ m/s, $Fr = 2.267$)

Run No.	L (cm)	t_{d0} (min)	t_{f0} (min)	t_{f0}/t_{d0}	t_0 (min)	d_{se-dig} (cm)	$d_{se-fill}$ (cm)	Δd_s (%)	Δd_h (%)	No. of flipping cycles
16	0	--	--	0	None	14.7	--	--	--	--
22	1	990	158	0.16	1149	13.8	10.4	25	-17	23 for 18 days
21	3	1612	737	0.46	2349	12	8	33	7	12 for 22 days
20	9	711	386	0.54	1097	9.6	5.2	46	21	8 for 7 days
15	15	332	604	1.82	936	8.1	5.1	37	41	9 for 7 days
13	21	40	217	5.43	257	6.5	4.6	29	47	41 for 7 days
14	30	2	21	10.50	23	3.9	2.8	28	14	70 for 2 days
161	35	--	--	0	None	--	--	--	--	--
162	40	--	--	0	None	--	--	--	--	--

Table 4.2 shows the summary of experimental data for all chosen Runs. For Runs 15, 13 and 14 which had longer apron length from 15 to 30 cm, the filling time was much longer than the digging time. According to the data, when the apron length became larger, the digging time decreases at a higher rate than the filling time over the recording period. Hence, more cycles were observed at a longer apron length and it could be as high as 35 cycles per day (Run 14).

As for shorter apron length, Runs 20, 21 and 22, where apron length was between 1 cm and 9 cm, the filling time was shorter than the digging time. When there was no apron and apron was longer than 35 cm (Runs 161 and 162), jet flipping phenomenon did not occur throughout the entire experiment.

Figure 4.6 shows the relationship between the ratio of average filling to digging time and the apron length ratio (L/d_o). This figure shows there are two critical apron lengths ratio, L_1/d_o and L_2/d_o that will affect the duration of digging and filling as well as the occurrence of jet flipping. When apron length ratio beyond $L_2/d_o = 35$, the effect of scouring was weak because of the long apron and no jet flipping was observed. This region is represented by the dash line, with $t_{f0}/t_{d0} = 0$ in Figure 4.6. For apron length ratio that is between L_1/d_o and L_2/d_o , the filling time was always lengthier than digging time, e.g. Runs 13, 14 and 15. Based on the graph, L_1/d_o is equal to 13.8 for $t_{f0}/t_{d0} = 1$ and when $L/d_o < 13.8$, the filling time is always shorter than the digging time and vice versa. More experiments should be conducted for $30 < L/d_o < 35$ to establish the trend line.

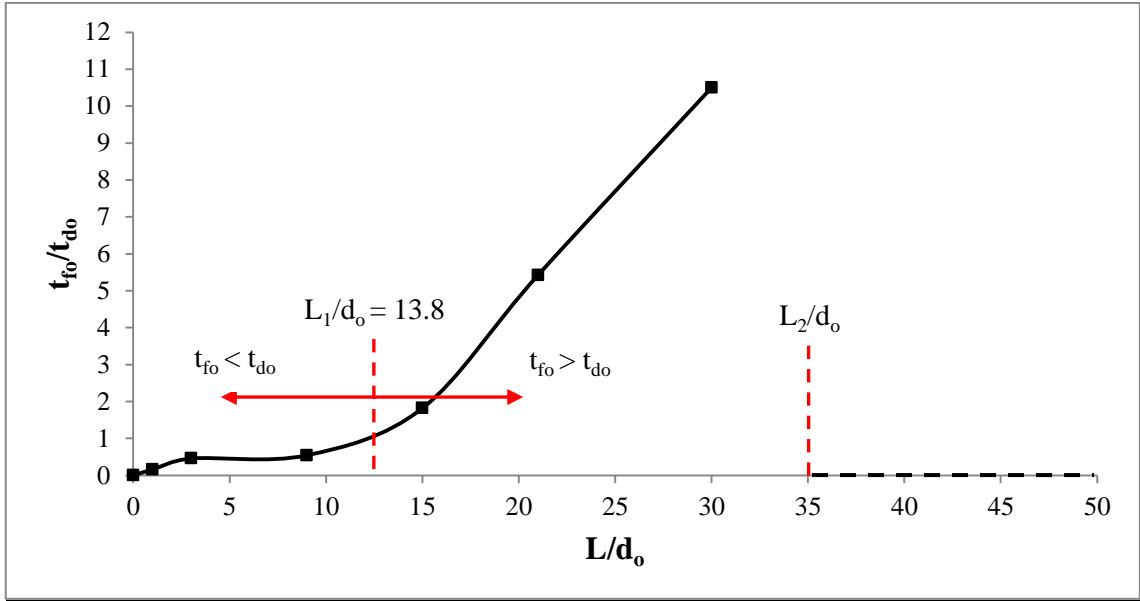


Figure 4.6 Relationship of the ratio of the average digging to filling time, t_{fo}/t_{do} versus apron length ratio, L/d_o

Figure 4.7 shows the relationship between t_o , i.e. the average time to complete one full dig-fill cycle and the apron length ratio L/d_o . From the figure, $L/d_o = 3$ is a critical value that divides the profile into 2 zones. For $L/d_o < 3$, the duration to complete one full dig-fill cycle is longer as the apron length ratio increases. However, this trend does not continue after $L/d_o > 3$, in fact, the duration to complete one full dig-fill cycle becomes shorter when the apron length ratio increases and reduces to zero when $L/d_o = 35$, with no occurrence of jet flipping.

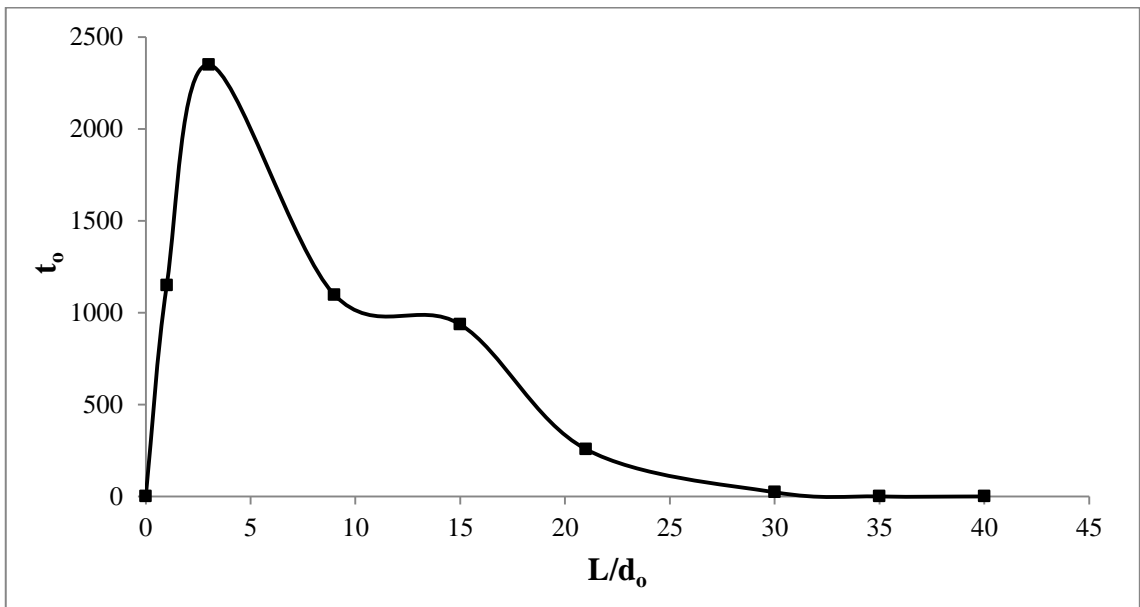


Figure 4.7 Relationship between t_o , average time to complete one full dig-fill cycle and the apron length ratio, L/d_o

4.3 Maximum and Minimum Scour Depth

Runs 13, 14, 15, 20, 21, 22 were selected to investigate the impact of apron length on scour depth and Runs 13, 18 and 81 were chosen to study the effect of flowrate on scour depth.

Figure 4.8 shows the changes of scour depth in the digging phases with respect to time in semi-log scale for Runs 20, 21 and 22. From this figure, it can be seen that the scour depth increases with time. However, the trends of the increase are different between the first cycle and subsequent cycles. This difference can be explained by comparing the scour profile at the commencement of first digging phase and the subsequent digging phases. The first digging phase started from a flat sand bed, i.e. no scour depth at the start of the run. However, the subsequent digging cycles began from the minimum scour depth, $d_{se-fill}$ position achieved from the previous cycles' filling phase. This had led to the formation of a gap in the changes of scour depth between the first digging phase and subsequent digging phases. Though, at the end of each phase, the scour depth would reach a maximum depth, d_{se-dig} and this value remained relatively constant throughout all the digging cycles in the experiment. This value indicates the maximum capability of the water in the digging process under this set of hydraulic parameters and the d_{se-dig} would be different for different Runs. In Figures 4.8, the maximum scour depth at equilibrium state during the first digging phase, $d_{lse-dig}$ is used to calculate the dimensionless maximum scour depth, $d_{st-dig}/d_{lse-dig}$.

Figure 4.9 illustrates the changes of scour depth in the filling phases with respect to time for Runs 20, 21 and 22. Based on the graphs, the scour depth reduces during the filling phase. Hence, it has proven that the scour hole is filled by the sand particles from sand ridge which is located downstream. The trend of decreasing in scour depth is the same throughout all cycles. The minimum scour depth, $d_{se-fill}$ was almost the same for each filling phase. In Figure 4.9, the minimum scour depth at equilibrium state during the first filling phase, $d_{lse-fill}$ is used to calculate the dimensionless minimum scour depth, $d_{st-fill}/d_{lse-fill}$.

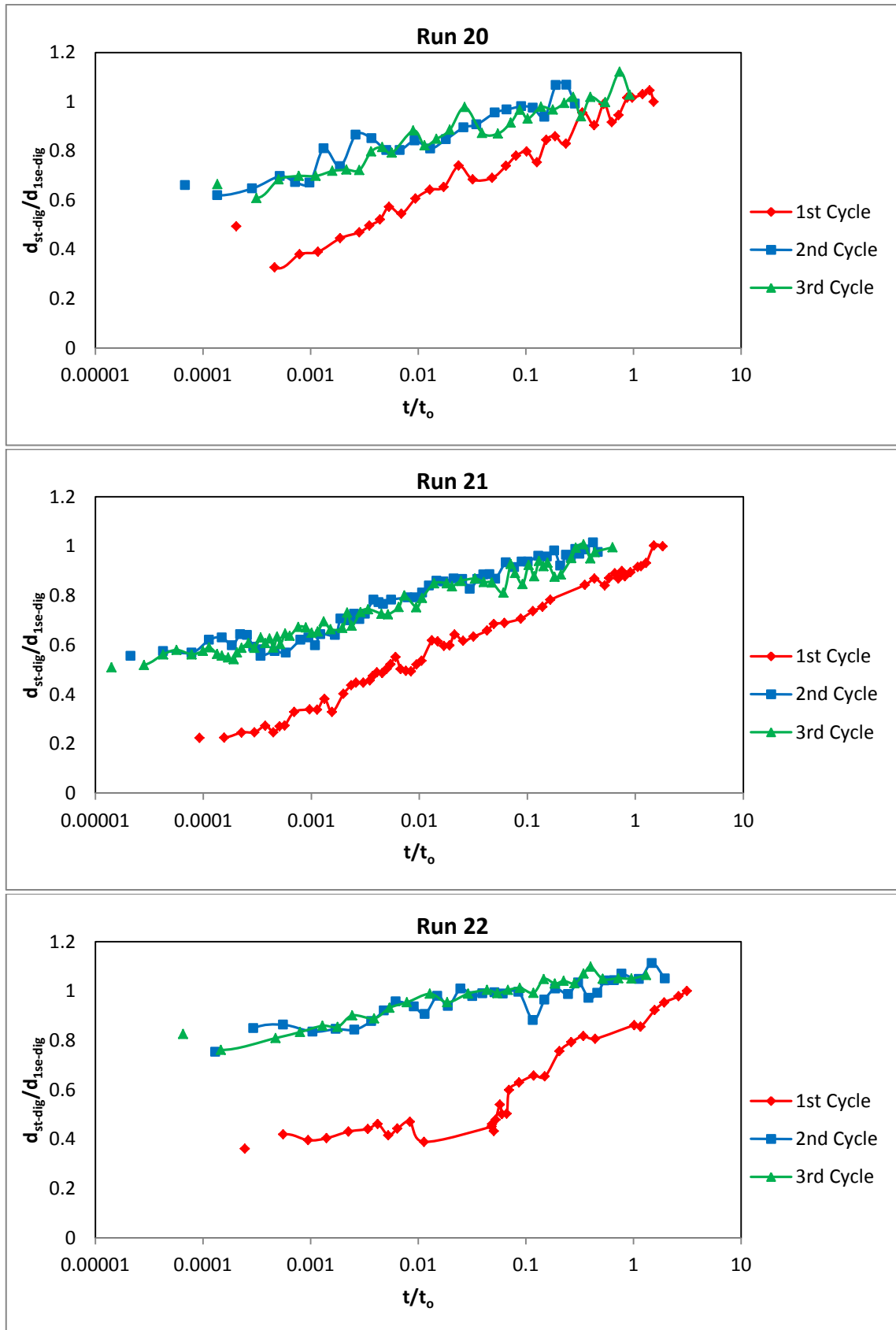


Figure 4.8 Relationship between ratio of scour depth (d_{st-dig}) to equilibrium scour depth ($d_{1se-dig}$) and ratio of digging duration for each cycle (t) to t_0 for Runs 20, 21, 22

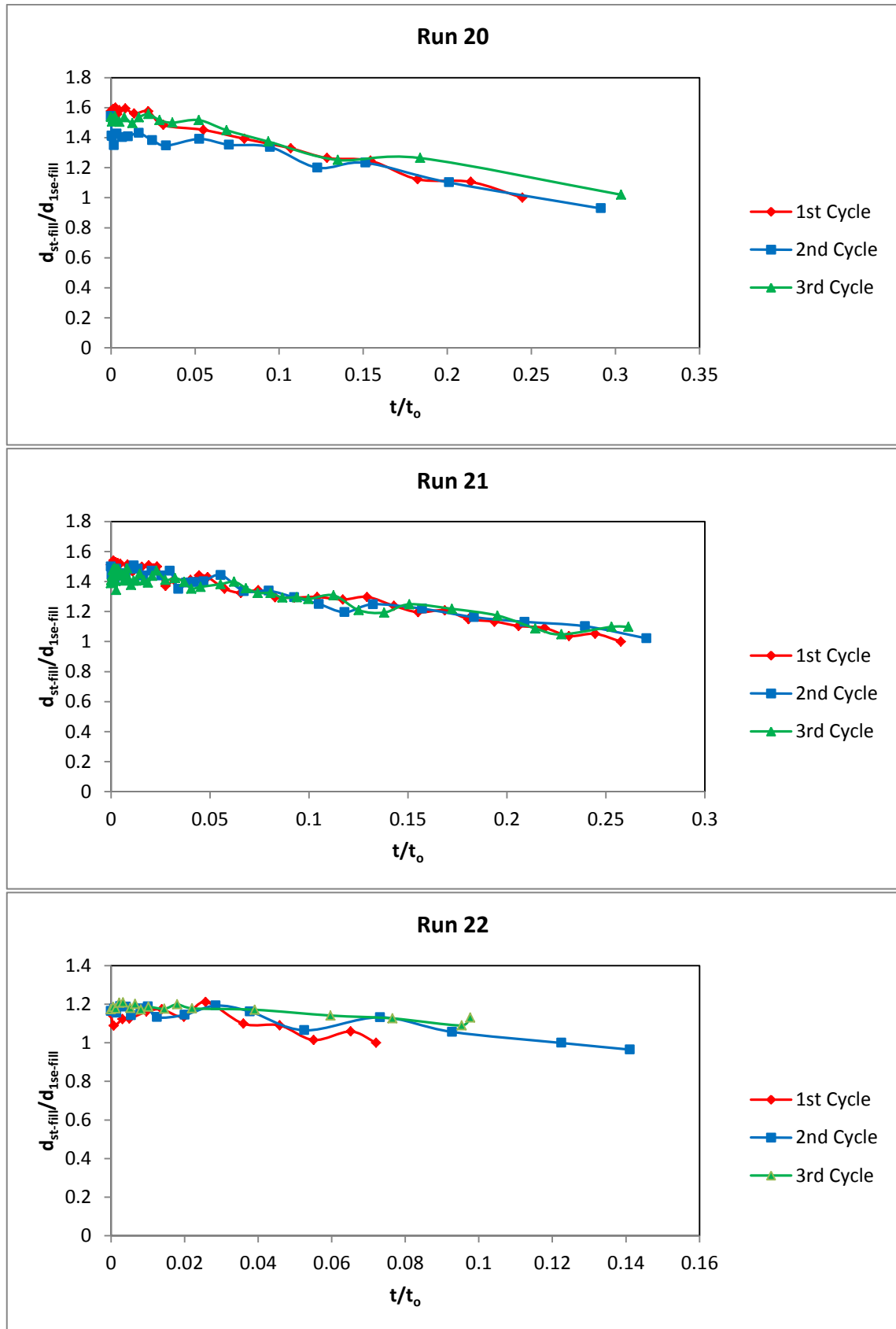


Figure 4.9 Relationship between ratio of scour depth ($d_{st-fill}$) to equilibrium scour depth ($d_{lse-fill}$) and ratio of filling duration for each cycle (t) to t_0 for Runs 20, 21, 22

In Table 4.2, the relative scour depth, Δd_s is used to compare the percentage of scour depth difference in different Runs.

The relative scour depth, Δd_s is defined for the % scour depth difference, where

$$\Delta d_s = \frac{(d_{se-dig} - d_{se-fill})}{d_{se-dig}} \times 100 \quad (4.5)$$

By keeping other parameters (flowrate, Q , tailwater depth, H_t) constant, the effects of apron length ratio, L/d_0 on maximum and minimum scour depth as well as Δd_s are plotted in Figures 4.10 and 4.11. The results in Figure 4.10 show that the scour depths decrease with increasing apron length. In Figure 4.11, Δd_s is not affected as much by the change in apron length as Δd_s initially increases from $L/d_0 = 1$ to a maximum at $L/d_0 = 9$ but gradually decreases to reach a value almost the same as $L/d_0 = 1$ as L/d_0 increases to 30.

From Table 4.2, flowrate does not show a direct effect on maximum and minimum scour depth, where by increasing the flowrate, maximum and minimum scour depth can be increased or decreased as well. However, the data show that relative scour depth can be affected by flowrate. The relative scour depth for Run 18 ($Q = 2.5$ L/s), Run 13 ($Q = 2.128$ L/s) and Run 81 ($Q = 1.818$ L/s) are 45%, 29% and 17% respectively.

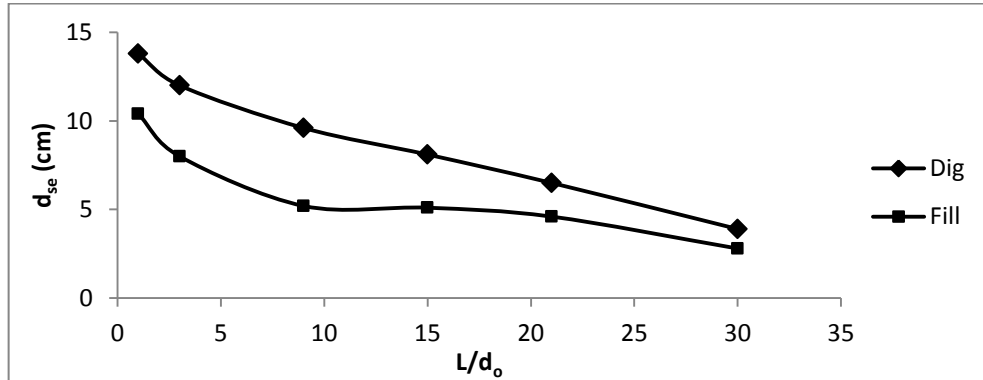


Figure 4.10 Effect of apron length ratio on maximum and minimum scour depth

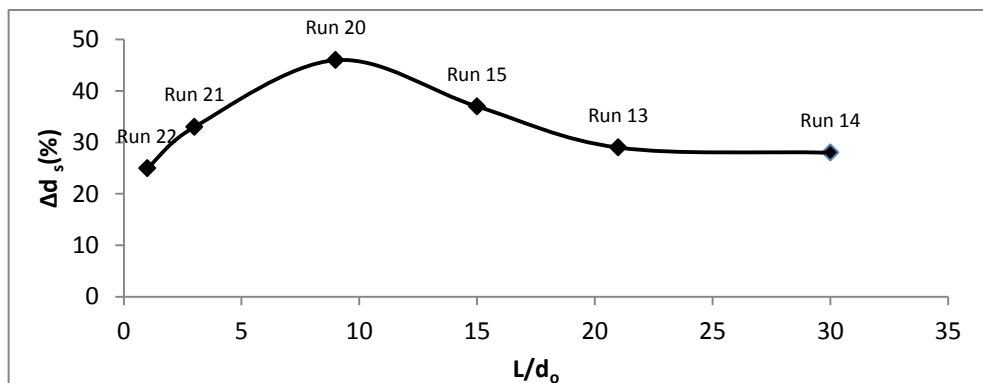


Figure 4.11 Effect of apron length ratio on Δd_s

4.4 The Observation of Sand Ridge

A sand ridge was formed downstream of the scour hole during the digging process. Observation showed that the formation and number of sand ridge were uncertain and mainly affected by the experiment conditions, especially the duration of digging and filling. The author had chosen Runs 21 and 13 for further discussion because the development and formation of sand ridge for these two Runs were varying widely.

In the following discussion, two different ridge heights (d_h) are used, d_{h2} and d_{h1} . The d_{h2} is defined as the height of ridge formed in the current cycle and d_{h1} is defined as the height of ridge formed from previous cycle or the 1st cycle. For example, the d_{h2} of first cycle will become the d_{h1} of the second cycle and the d_{h2} of second cycle become d_{h1} in the third cycle and so on.

Run 21 had the longest duration of one full dig-fill cycle compare with other Runs (see Table 4.2). In Figure 4.12, the development of ridge height for the first three dig-fill cycles in Run 21 is plotted against time. The formation and changes of sand ridge in Run 21 was the most typical case where two sand ridges were formed in each cycle except the first cycle. The sand ridge formed in the first cycle (blue line) did not disappear, but reduced in height. The newly formed sand ridge (red line) for each cycle did not merge with the sand ridge formed in the first cycle. It had been noticed that the height of ridge will increase in the initial stage of the filling phase; this phenomenon will be explained in detail in Section 4.4.1. In Figures 4.12 and 4.13, ridge height at the equilibrium state during the first digging phase, d_{1H-dig} is used to calculate the dimensionless ridge height, d_h/d_{1H-dig} .

On the other hand, Run 13 had a much shorter duration of one full dig-fill cycle than Run 21. In Run 13, most of the time only single sand ridge was observed (see Figure 4.13). At the beginning of the second filling phase, d_{h2} was much higher than d_{h1} , however, after sometimes of filling, the current d_{h2} overtopped on d_{h1} formed from the previous cycle and d_{h1} reduced to zero (black dotted circle in Figure 4.13). On the other hand, in the third filling phase, the current d_{h2} merged below d_{h1} formed from the previous cycle and d_{h2} reduced to zero (black circle in Figure 4.13). This situation was totally different from the second filling phase. Figures 4.14 and 4.15 give a clearer image on the formation of sand ridge that stated earlier.

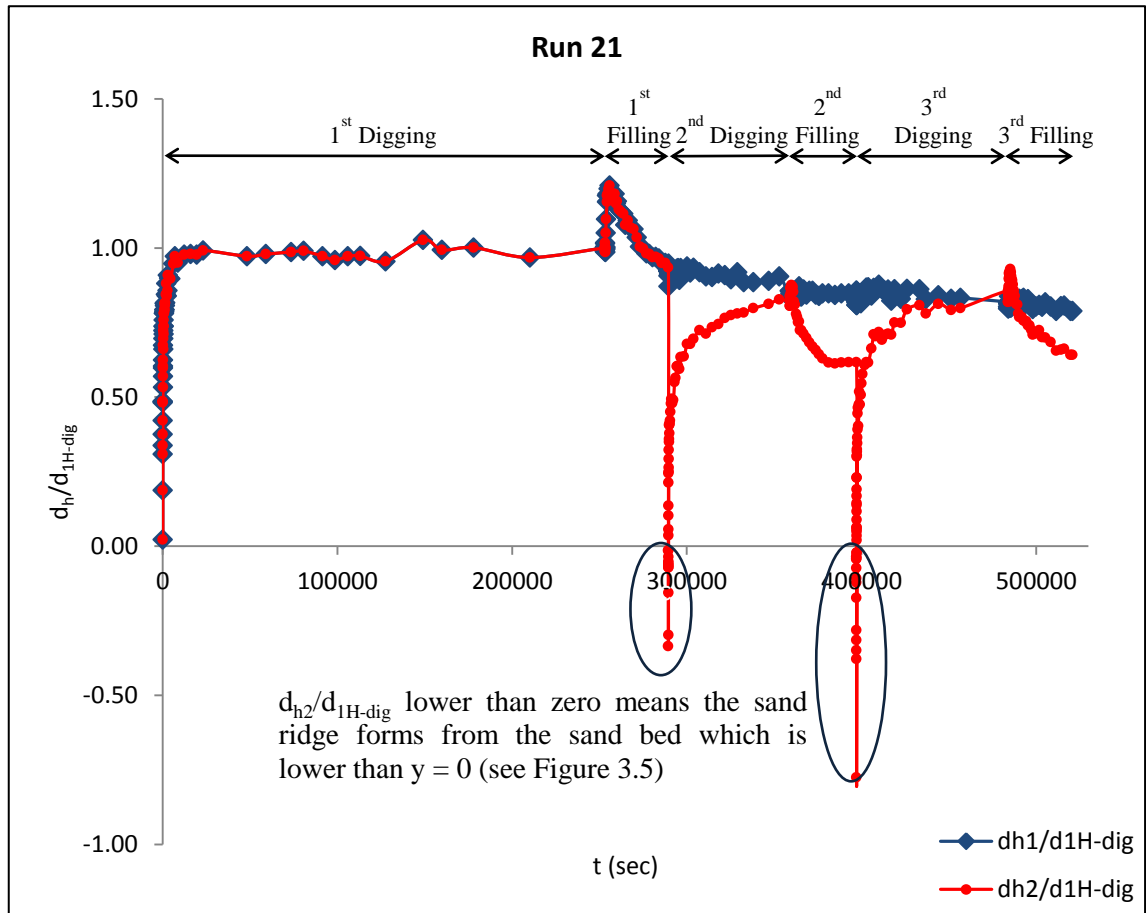


Figure 4.12 Development of sand ridge in the first 3 dig-fill cycles for Run 21

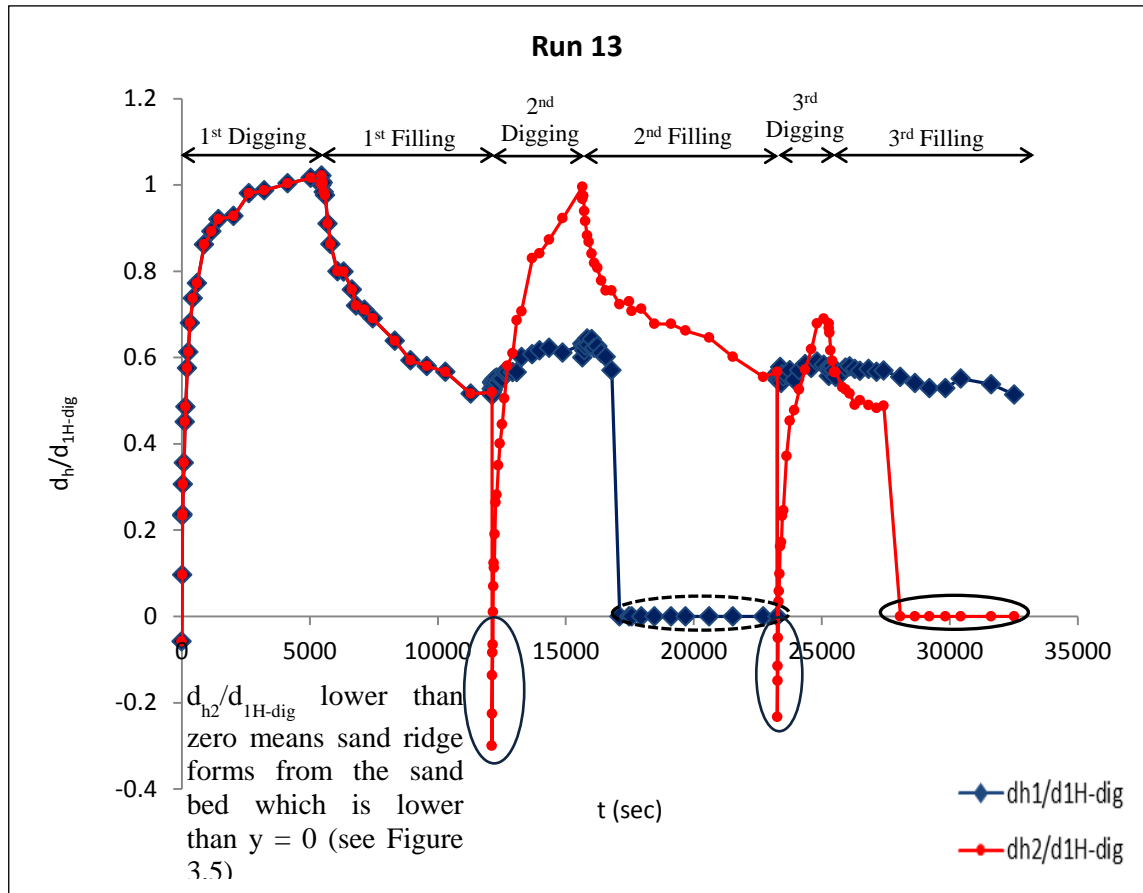


Figure 4.13 Development of sand ridge in the first 3 dig-fill cycles for Run 13

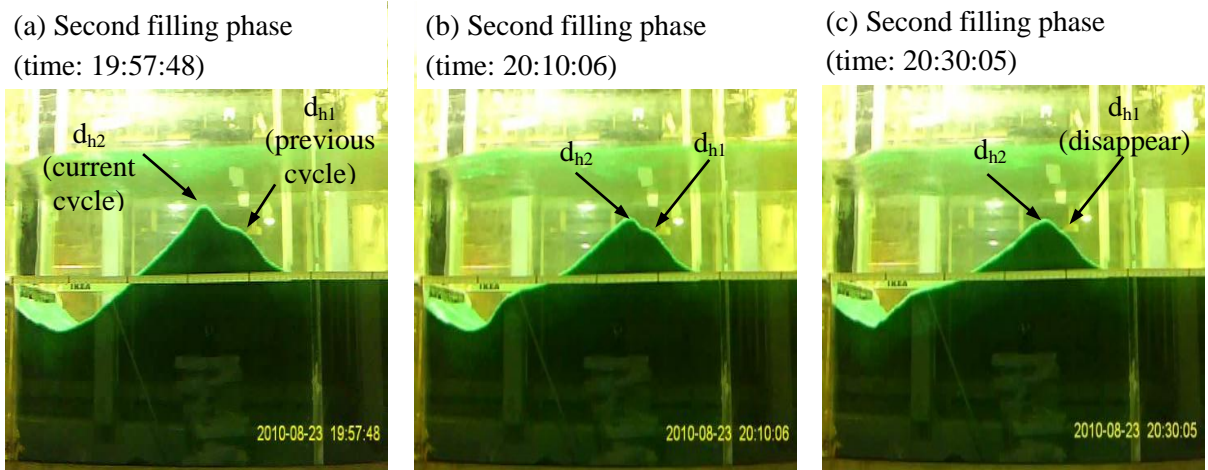


Figure 4.14 Run 13: Sequence of the current d_{h2} formation overtopping on d_{h1} formed from previous cycle

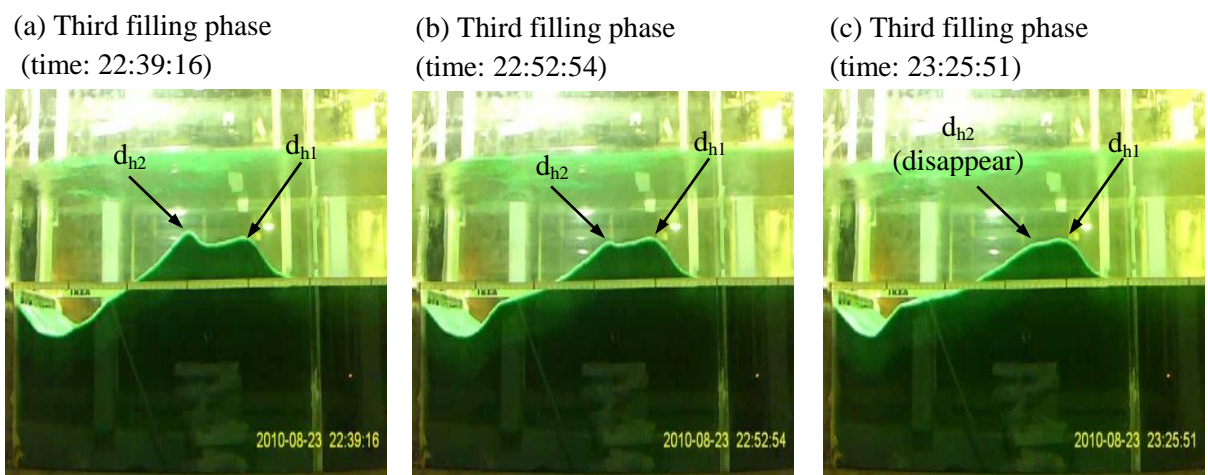


Figure 4.15 Run 13: Sequence of the current d_{h2} formation merging below d_{h1} formed from previous cycle

4.4.1 Effect of Apron Length on Height of Ridge

In Section 4.4, two kinds of ridge height, d_{h1} and d_{h2} were introduced and used to describe the formation and changes of sand ridge. In this section, only the height of ridge that formed in the current cycle, d_{h2} will be used to carry out the investigation of ridge height under different apron length and the same Runs in Section 4.3 were used.

Figures 4.16 and 4.17 indicate the changes of ridge height in the digging and filling phases with respect to time, ridge height at the equilibrium state during the first digging and filling phase, d_{1H-dig} and $d_{1H-fill}$ are used to calculate the dimensionless ridge height, d_{h2}/d_{1H-dig} and $d_{h2}/d_{1H-fill}$. In Figure 4.16, the difference in the increasing trend between the first digging phase (1st cycle) and the later digging phases (2nd and 3rd cycle) is observed. This could be explained by the amount of sand particles in the first digging phase was more than others. When the filling phase occurred, only a portion of sand particles in the sand ridge was being filled back to the scour hole, therefore, it created the disparity in the amount of sand particles in the first and other digging phase. Thus the formation of gap in Figure 4.16 was due to the first digging phase had more sand particles to be pushed.

By observing Figure 4.17, for Runs 21 and 20, the height of ridge increases at the beginning of filling phase before it sinks. By referring to Figure 4.2, the backward movement of the sand is being dragged by the flow in the second recirculation region (dark blue line). The impingement point in this flow region is located half way on the sand ridge (red circle in Figure 4.2), and it initiates the sand particle movement in upper and lower parts of the sand ridge in two opposite directions, upward and downward respectively. At the beginning of filling phase, the ridge height continued to growth. However, after a period of time, the height decreased because the sand particles in lower part of the ridge had been moved back to the scour hole. At the same time, the sand particles in upper part rolled downwards to fill the sand lost in lower part. However, the situation in Run 22 was different, the ridge height was observed to increase throughout the whole filling process. By referring to Table 4.2, the total filling duration for Run 22 is around 158 min which is lower than Runs 20 (386 min) and 21 (737 min). Therefore, it might be insufficient time for the sand in upper part to roll back.

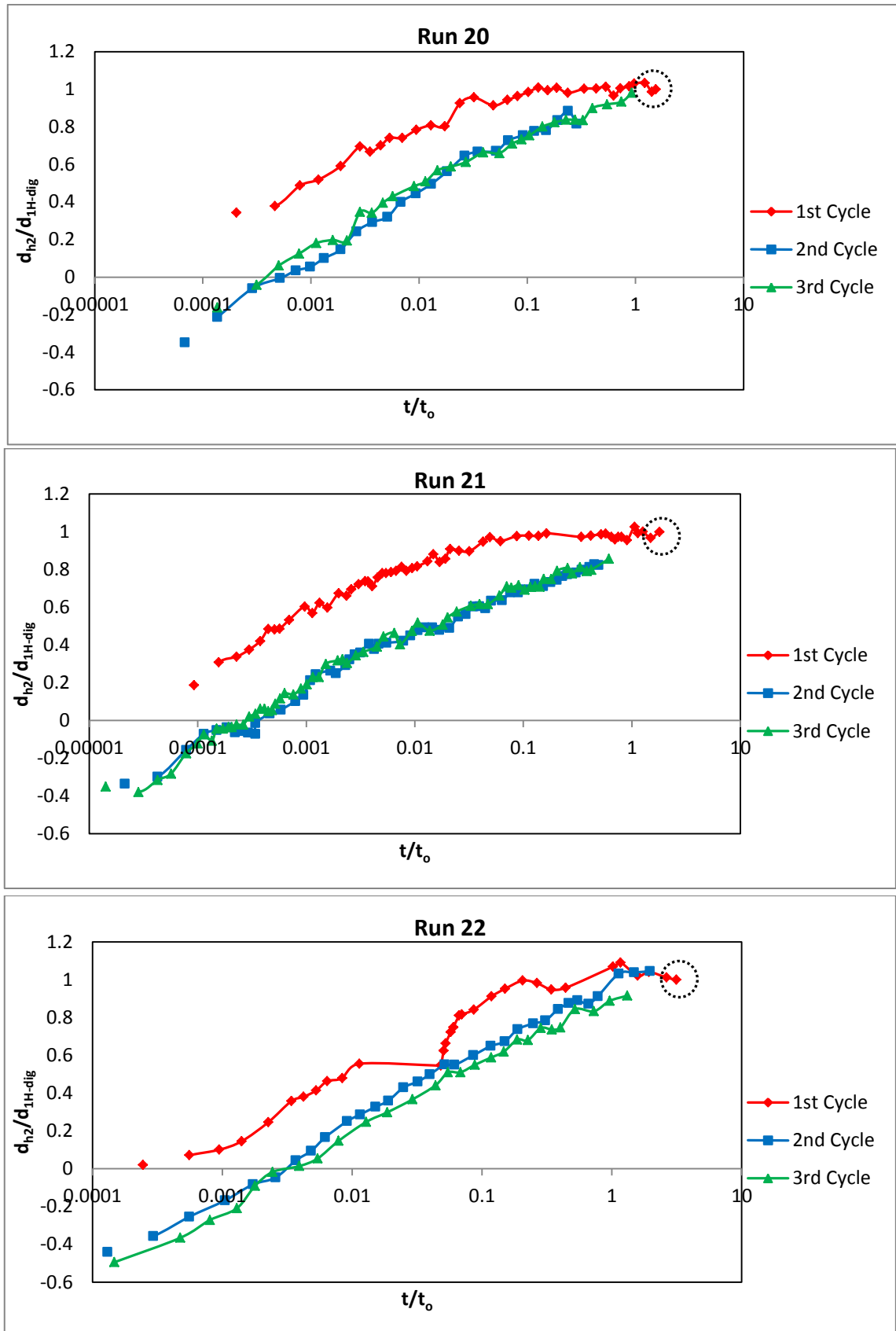


Figure 4.16 Relationship between ratio of ridge height (d_{h2}) to equilibrium ridge height (d_{1H-dig}) and ratio of digging duration for each cycle (t) to t_0 for Runs 20, 21, 22

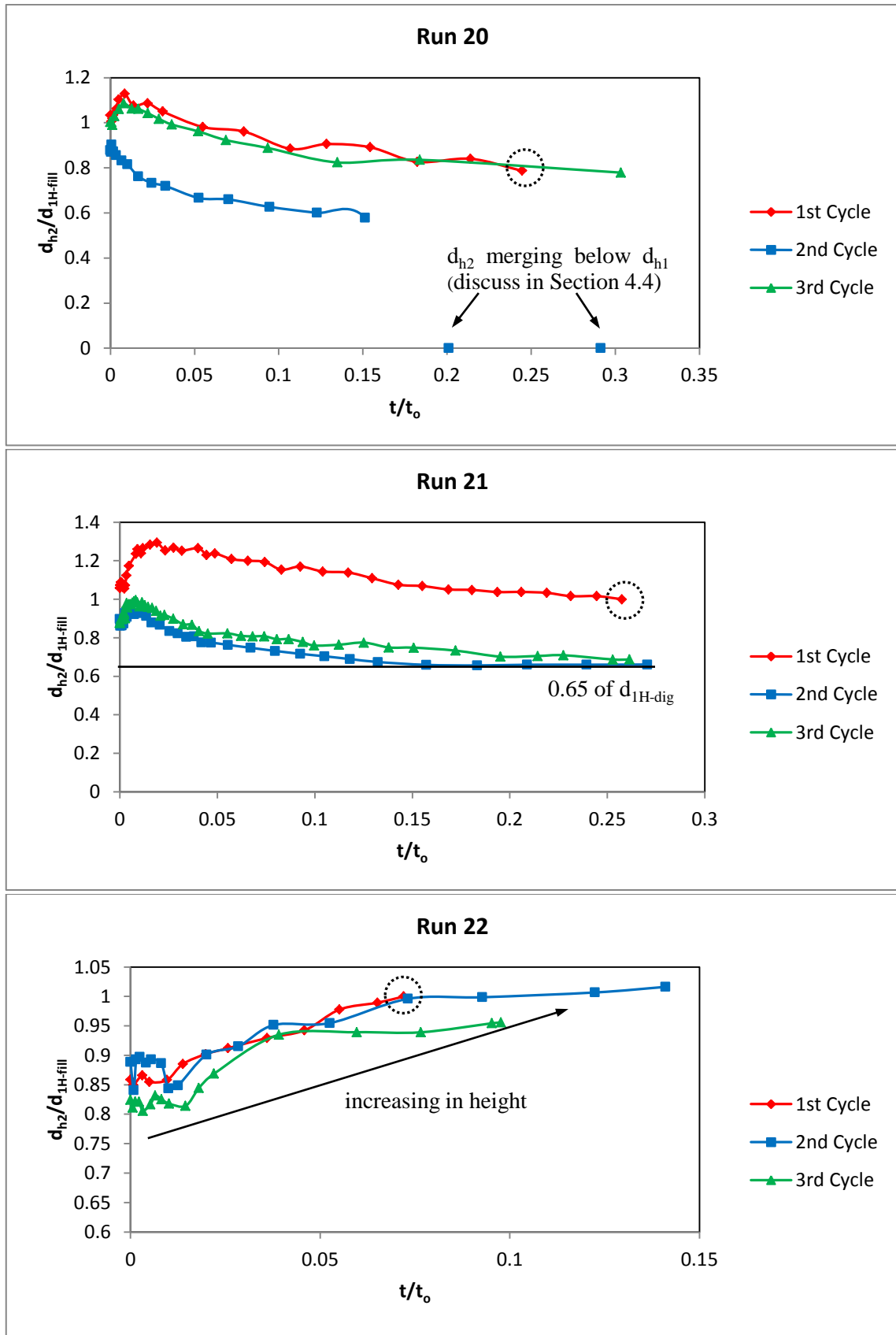


Figure 4.17 Relationship between ratio of ridge height (d_{h2}) to equilibrium ridge height ($d_{IH-fill}$) and ratio of filling duration for each cycle (t) to t_0 for Runs 20, 21, 22

By modifying Eq 4.5, the percentage of ridge height difference, Δd_h can be calculated, where

$$\Delta d_h = \frac{(d_{1H-dig} - d_{1H-fill})}{d_{1H-dig}} \times 100 \quad (4.6)$$

The ridge height at the equilibrium state in the first digging or filling phase is used instead of average ridge height; this is because normally the ridge height in the first phase is the highest. This can be seen from the dotted circles in Figures 4.16 and 4.17.

Figure 4.18 represents the percentage of ridge height difference (Δd_h) against apron length ratio (L/d_o). From the figure, in the region where L/d_o is smaller than 2, negative Δd_h is observed which means the ridge height in filling phase is higher than digging phase. However, for other L/d_o , higher ridge height in digging phase is recorded. The difference in the ridge height caused by apron length is quite significant, from -17% (Run 22) to 47% (Run 13).

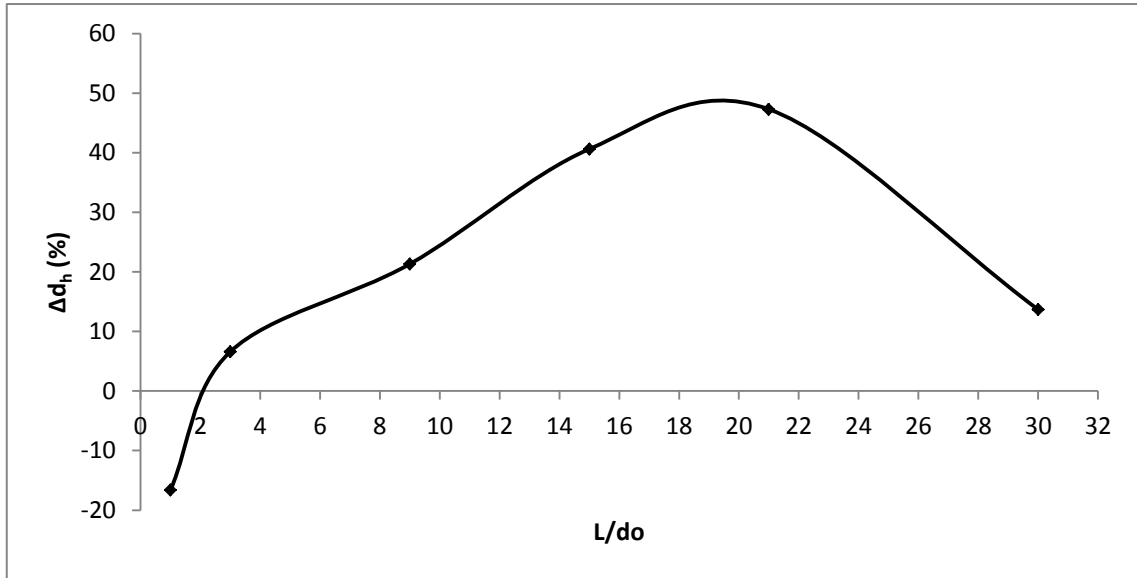


Figure 4.18 Effect of apron length ratio on Δd_h

4.5 Effect of Different Parameters on the Occurrence of Jet flipping

The occurrence of jet flipping is affected by parameters such as tailwater depth, flowrate and apron length individually while other parameters are constant. Most of the researchers found that jet flipping only occurred in shallow tailwater depth (Ali and Lim 1986; Johnston 1990; Balachandar and Kells 1997; Deshpande, Balachandar et al. 2007). However in the present study, it was discovered jet flipping also occur with large tailwater depth. In addition, it was found that flowrate and apron length were another parameters that would affect the occurrence of jet flipping. But, the distinctions between high and low flowrate as well as long and short apron length have not been clearly defined.

In Figure 4.6, when tailwater depth ($H_t = 12.7$ cm), sluice gate opening ($d_o = 10$ mm), discharge ($Q = 2.128$ L/s), velocity ($u_o = 0.71$ m/s), Froude number ($Fr = 2.267$) remain unchanged, a critical range of apron length ratio (L/d_o) between 30 and 35 may influence the occurrence of jet flipping.

Runs 121 and 85 as well as Runs 79 and 85 were used to find out the critical range of flowrate and tailwater depth respectively. All these Runs were carried out in the condition of high submergence or large tailwater depth ($H_t = 16$ cm and 12.7 cm) and 90 mm of apron length (see Table 4.1).

4.5.1 Effect of Tailwater Depth

Runs 79 and 85 were conducted in high submergence manner, but jet flipping only occurred in Run 79 that had tailwater depth of 12.7 cm. Therefore there must be a critical range of tailwater depth that would affect the occurrence of jet flipping. The procedure is discussed in detail in this section.

First, $H_t = 13.5$ cm was chosen to conduct the experiment (Run 79 ($H_t = 13.5$ cm)). Bases on Figure 4.19, the first digging phase in Run 79 consumes 3854 minutes, which is around 2 days. As a result, 8 days (4 times higher than 2 days) was chosen as the time limit to observe the jet flipping phenomenon. After 8 days of experiment, no jet flipping was observed and the author stopped the experiment.

Next another tailwater depth which was in the range from 12.7 cm to 13.5 cm was chosen to conduct the following experiments. In order to narrow the range, this process was repeated a few times until the range was lower to an acceptable level. A range of 0.5 cm was selected as the acceptable level. In conclusion, with apron length, $L = 90$ mm; flowrate, $Q = 1.818$ L/s; jet

flipping will occur when the tailwater depth is between 12.7 cm and 13 cm, whereas it will not occur when tailwater depth is between 13.5 cm to 16 cm. The summary of Run 79 is listed in Table 4.3.

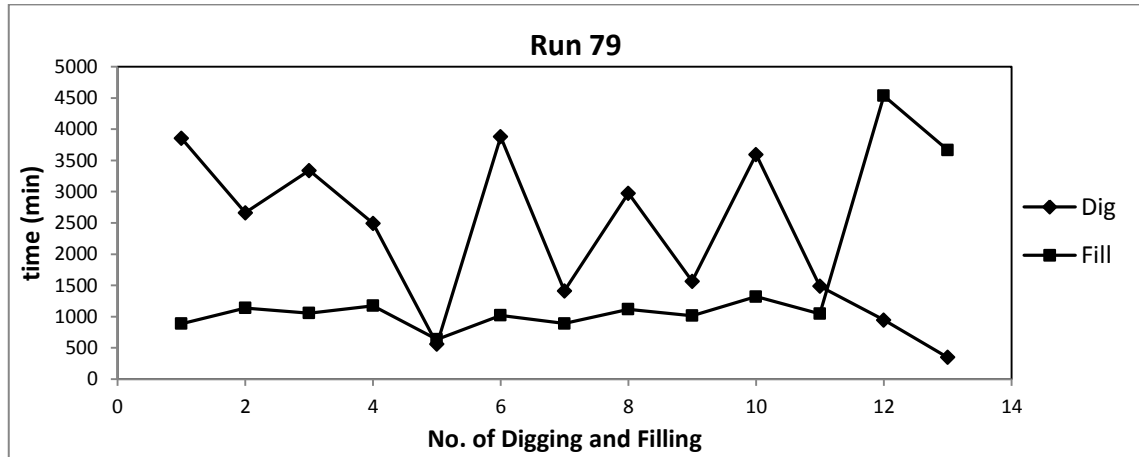


Figure 4.19 Time-sequence of each digging and filling phase for Run 79

4.5.2 Effect of Flowrate

In Table 4.3, Run 121 was conducted for 12 days and 12 cycles were observed. However for Run 85, all the parameters were similar to Run 121 except for the flowrate, $Q = 1.818$ L/s, and no jet flipping was observed. Therefore there must be a critical range of flowrate that would affect the occurrence of jet flipping. The procedure is discussed in detail in this section.

First, the average value of 2.2 L/s for 2.5 L/s and 1.818 L/s was used to conduct the first experiment (Run 121 ($Q = 2.2$ L/s)). Based on Figure 4.20, the duration of the first digging phase in Run 121 is 4276 minutes, which is nearly 3 days. Therefore, 8 days (about 2.7 times higher than 3 days) was chosen as the time limit to observe the occurrence of jet flipping. After 8 days of continuous experiment, no jet flipping was observed and the experiment was stopped.

Next, another flowrate was chosen which was in the range from 2.5 L/s to 2.2 L/s to conduct the following experiments. In order to narrow the range, this process was repeated a few times until the range is lower to an acceptable level. Due to time constraint, the author has selected a range of 0.1 L/s as the acceptable range. In conclusion, with apron length, $L = 90$ mm; tailwater depth, $H_t = 16$ cm; flowrate, $Q = 2.2$ L/s to 2.3 L/s is the critical range of flowrate, above which jet flipping occurred and below which no jet flipping would happen.

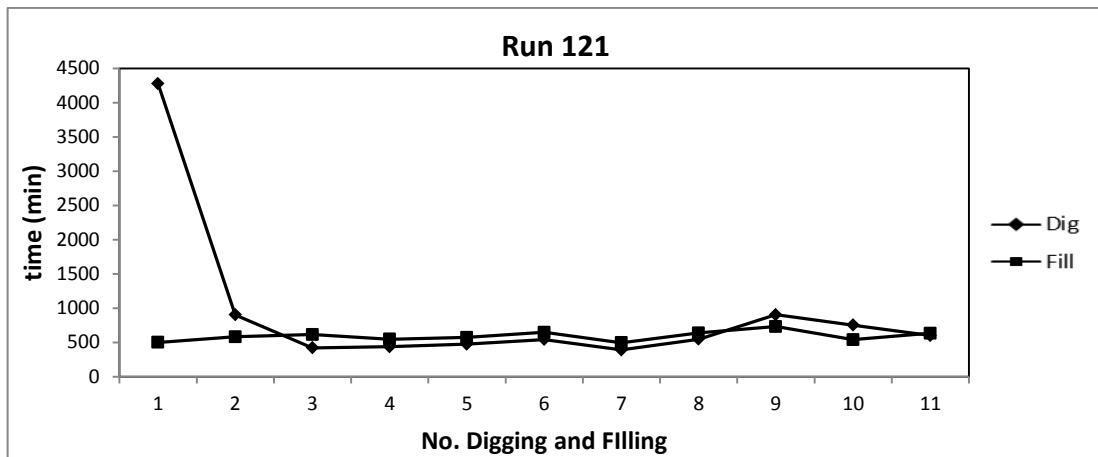


Figure 4.20 Time-sequence of each digging and filling phase for Run 121

The summary of the data for the procedures in Sections 4.5.1 and 4.5.2 are listed in Table 4.3, set 1 and 2. From the data, by increasing the tailwater depth or increase the flowrate of Run 85, a threshold of jet flipping can be established, even under high submergence. More experiments need to be conducted to produce a demarcation diagram for the threshold of jet flipping as a function of the flowrate, tailwater depth and apron length.

Table 4.3 Summary of data

	Run	do (mm)	L (mm)	Q (L/s)	Ht(cm)	Uo (m/s)	F ₀	F _r	Progress/result	Duration
Set 1	79	10	90	1.818	12.7	0.606	5.575	1.935	Flipping occur	28 days
	79 (Ht=13)	10	90	1.818	13	0.606	5.575	1.935	Flipping occur	9 days
	79 (Ht=13.5)	10	90	1.818	13.5	0.606	5.575	1.935	No flipping	8 days
	79 (Ht=14)	10	90	1.818	14	0.606	5.575	1.935		
	79 (Ht=15)	10	90	1.818	15	0.606	5.575	1.935		
	85	10	90	1.818	16	0.606	5.575	1.935	No flipping	15days

	Run	do (mm)	L (mm)	Q (L/s)	Ht (cm)	Uo (m/s)	F ₀	F _r	Progress/result	Duration
Set 2	121	10	90	2.5	16	0.833	7.666	2.661	Flipping occur	12 days
	121 (Q=2.45)	10	90	2.45	16	0.817	7.516	2.610	Flipping occur	8 days
	121 (Q=2.4)	10	90	2.4	16	0.800	7.360	2.556	Flipping occur	7 days
	121 (Q=2.3)	10	90	2.3	16	0.767	7.056	2.450	Flipping occur	17 days
	121 (Q=2.2)	10	90	2.2	16	0.733	6.743	2.342	No flipping	8 days
	121 (Q=2.1)	10	90	2.1	16	0.700	6.440	2.236		
	121 (Q=2)	10	90	2	16	0.667	6.136	2.131		
	121 (Q=1.9)	10	90	1.9	16	0.633	5.823	2.022		
	85	10	90	1.818	16	0.606	5.575	1.935	No flipping	15 days

CHAPTER 5 CONCLUSIONS

This study investigates the jet flipping and scouring characteristics for a submerged jet below a sluice gate and the conclusions are as follows:

1. It was found in the initial period, the jet issuing from the sluice gate impinges on the sand bed and the rate of scour development during this digging phase was rapid. Then the rate of scour slowed down and finally reached a pseudo equilibrium stage with no observable changes in the bed profile as time progresses. This is the bed jet phase where the jet attaches completely to the bed and digging it to a maximum scour depth, d_{se-dig} .
2. Depending on a certain combination of the tailwater depth, jet discharge and apron length, it was observed that the bed jet would suddenly flip towards the water surface forming a surface jet phase. During this phase, the jet would erode the sand ridge in a reverse direction causing sand particles to be transported back into the scour hole. The rate of filling was relatively stable, and the filling phase stopped when it reached a minimum scour depth, $d_{se-fill}$. The jet would then almost instantaneously revert back to a bed jet phase. The jet-flipping and its associated digging and filling processes are cyclical and repeated many times over the long scouring duration used in this study.
3. The results on the effect of the apron length on the jet flipping phenomenon showed that the duration of the filling phase is generally longer than the digging phase with longer apron length. The duration to complete one dig-fill cycle also decreases with increases in apron length.
4. For apron length as a ratio of the jet opening, L/d_o greater than 35, there is no jet flipping and only bed jet was observed. Similarly, when there is no apron, i.e., L/d_o is equal to zero, there is no jet flipping in the scour hole.
5. Based on the results, it was found that generally the maximum scour depth, d_{se-dig} during the digging phase and minimum scour depth, $d_{se-fill}$ during the filling phase increase as the apron length decreases. The difference between the d_{se-dig} and $d_{se-fill}$ is larger with increases in jet discharge.
6. At the downstream of the scour hole, the sand ridge formed is affected by the cyclical digging and filling action. There are two sand ridges formed with different heights during the dig-fill cycles. For apron length ratio, L/d_o lower than 2, the height of sand ridge during the filling phase is higher than that during the digging phase.
7. Preliminary results on the threshold of jet-flipping with respect to a range of tailwater depths and jet discharges rates showed that for a particular apron length ratio and jet

discharge, there is a critical tailwater whereby jet flipping will not occur if its value is above the critical value and vice versa. Similarly for a particular apron length ratio and tailwater, there is a critical jet discharge such that jet flipping will occur if its value is higher than the critical value and vice versa.

REFERENCES

- [1] Ali, K. H. M. and Lim, S. Y. (1986). "Local Scour Caused by Submerged Wall Jets." Proceedings ICE **81**(4): 607–645.
- [2] Balachandar, R. and Kells, J. A. (1997). "Local channel in scour in uniformly graded sediments: the time-scale problem." Canadian Journal of Civil Engineering **24**(5): 799-807.
- [3] Bey, A., Faruque, M. A. A., et al. (2007). "Two-Dimensional Scour Hole Problem: Role of Fluid Structures." Journal of Hydraulic Engineering ASCE, **133**(4): 414-430.
- [4] Deshpande, N., Balachandar, R., et al. (2007). "Effects of submergence and test startup conditions on local scour by plane." Journal of Hydraulic Research **45**(3): 370-387.
- [5] Dey, S. and Sarkar, A. (2007). "Effect of Upward Seepage on Scour and Flow Downstream of an Apron due to Submerged Jets." Journal of Hydraulic Engineering ASCE, **133**(1): 59-69.
- [6] Dey, S. and Westrich, B. (2003). "Hydraulics of Submerged Jet Subject to Change in Cohesive Bed Geometry." Journal of Hydraulic Engineering ASCE, **129**(1): 44.
- [7] Hoffmans, G. J. C. M. and Verheij, H. J. (1997). Scour manual / G.J.C.M. Hoffmans, H.J. Verheij, Rotterdam, Netherlands : A.A. Balkema, 1997.
- [8] Johnston, A. J. (1990). "Scourhole developments in shallow tailwater." Journal of Hydraulic Research **28**(3): 341-354.
- [9] Karim, O. A. and Ali, K. H. M. (2000). "Prediction of flow patterns in local scour holes caused by turbulent water jets." J. Hydraul. Res. **38**(4): 279-287.
- [10] Kurniawan, A. and Altinakar, M. S. (2002). "Velocity and Turbulence Measurements in a Scour Hole Using an Acoustic Doppler Velocity Profiler." Third ISUD for fluid mechanics and fluid engineering (EPFL): 37-43.

- [11] Lim, S. Y. and Xie, C. (2011). JObservations on Jet-Flipping in Localized Scour by 2-D Wall Jets. Proc. 34th IAHR World Congress, 26 June - 1 July, 2484-2491.
- [12] Lim, S. Y. and Chiew, Y. M. (2001). Erosion Below Tidal Sluice Gate. Research Report, Sch of CEE, NTU.
- [13] Ling, Q. (2011). Jet-Flipping Phenomenon Under Sluice Gate. FYP Report, Sch of CEE, NTU
- [14] Nik Hassan, N. M. K. and Narayanan, R. (1985). "Local Scour Downstream of an Apron." Journal of Hydraulic Engineering ASCE, **111**(11): 1371-1385.
- [15] Rajaratnam, N. (1981). "Erosion by Plane Turbulent Jets." Journal of Hydraulic Research **19**(4): 339-358.
- [16] Rajaratnam, N. and Macdougall, R. K. (1983). "Erosion by Plane Wall Jets with Minimum Tailwater." Journal of Hydraulic Engineering ASCE, **109**(7): 1061-1064.